Analysing the change in water quality parameters along river Ganga at Varanasi, Mirzapur and Ghazipur using Sentinel-2 and Landsat-8 satellite data during pre-lockdown, lockdown and post-lockdown associated with COVID-19

Nilendu Das, Rajarshi Bhattacharjee*, Abhinandan Choubey,
Ashwani Kumar Agnihotri, Anurag Ohri and Shishir Gaur

*Department of Civil Engineering, Indian Institute of Technology (BHU – Banaras Hindu University),
Varanasi 221 005, India.*
Corresponding author. e-mail: rajbhatt78645@gmail.com

The proper functioning of the river ecosystem has been symbolised by healthy aquatic life. The river Ganga has shown signs of rejuvenation due to lockdown. In this study, an attempt has been made to analyse the change in river water quality using Sentinel-2 and Landsat-8 imageries. The quantitative analysis has been performed for temperature and normalised difference turbidity index (NDTI). The qualitative analysis has been performed for pH, dissolved oxygen (DO) and total suspended solids (TSSs). Ghazipur, Varanasi and Mirzapur stretches have been selected for this study. In the Ghazipur stretch, the river temperature decreased by 7.14% in May 2020 (lockdown period) as compared to May 2019 (1 year before lockdown). Similarly, in the Varanasi stretch, this decrease has been by 8.62%, and in the Mirzapur stretch, this decrease has been by 12.06% in May 2020 compared to May 2019. For the same period, NDTI in the Ghazipur, Varanasi and Mirzapur stretch has been decreased by 0.22, 0.26 and 0.24, respectively. The pH and DO of the river increased, and TSS decreased for the considered time period. The lockdown during the second wave of the coronavirus disease 2019 was not helpful for river rejuvenation. This study elicited how the behaviour of the parameters changed during the lockdown.

Keywords. Lockdown; Varanasi; Ganga; Sentinel-2; Landsat-8; water quality.

1. Introduction

The mapping of the river or the inland water quality using remote-sensing technology was not new for the scientific community, and this activity has been practiced since the 1970s with the launch of the Landsat series of satellites (Klemas *et al.* 1971; Ritchie *et al.* 1976). The conventional procedures for testing the water quality parameters are expensive as well as time-consuming, and it provides information only for the point(s) under measurement. The remote-sensing technology can be utilised as an advantageous alternative option for the measurement of the water quality parameters. The remote-sensing-based satellite images can provide systematic and periodic coverage of an area. More information can be deduced for a place because of

the periodic nature of the satellite revisit (de Moraes Novo *et al.* 2006; Lamaro *et al.* 2013). Every feature of the earth's surface behaves uniquely while interacting with electromagnetic (EM) radiation. This distinctiveness generates in the form of the spectral signature from each surface feature, and this signature has been utilised to identify the surface feature through satellite images (Elachi 1987; Joseph 1996). When a slight change in the composition of a feature occurs, it simultaneously changes the spectral signature (Moore 1980). Several factors accompany the change of the spectral signature for a feature, and the same can be valid for the water feature. Some of the factors responsible for generating the different spectral signatures of water are the incidence angle of the sun, the season of the year, water surface roughness, turbidity, depth of the water and vegetation growth on the water surface (Garg *et al.* 2020). By studying these different spectral signatures, the qualitative and sometimes the quantitative assessment of a particular component can be accomplished (Chander *et al.* 2019; Luis *et al.* 2019). Several water-quality parameters such as temperature, turbidity, dissolved oxygen (DO), pH, total dissolved solids and total suspended solids (TSSs) can be studied with the help of remote-sensing technology (Lamaro *et al.* 2013; Khattab and Merkel 2014; El Din and Zhang 2017; Garg *et al.* 2020; Patel *et al.* 2020).

The temperature of the water is one of the significant parameters because it helps regulate the rate of chemical reactions in the river, and it also controls the DO concentrations along with the nutrient cycle of the aquatic creatures; thus, it influences the freshwater ecology (Caissie 2006; Wawrzyniak *et al.* 2012). The continuum concept of the river signifies that any change in the river temperature can intensely impact the longitudinal distribution of organisms in the fluvial ecosystem (Vannote *et al.* 1980; Wawrzyniak *et al.* 2012). The rise of the river temperature above a specific threshold hampers the biological processes such as growth, reproduction and survival rate of the aquatic species (Eaton *et al.* 1995; Xin and Kinouchi 2013). According to Vant's Hoff theory, it can be stated that for every 10°C rise in the temperature of water, the biological activity nearly doubles within the temperature range of 0–40°C under

normal situations (Gillooly *et al.* 2001; Caissie 2006). In comparison with the *in-situ* measurements, the remote-sensing techniques provide alluring possibilities for estimating and observing the river temperature as well the spatial thermal pattern of the river (Ling *et al.* 2017). Several researchers are now using remote-sensing technology for estimating the temperature of river water. The thermal bands present in the Landsat satellite system have been used for this purpose (Lamaro *et al.* 2013; Wawrzyniak *et al.* 2016).

Turbidity is another essential water quality parameter where suspended sediments, instead of transmitting the light along the water column they scatter light (Sebastiá-Frasquet *et al.* 2019). When the concentration of suspended solids or sediments in water increases, the turbidity is also enhanced, and higher turbidity values hamper the aquatic ecosystem (Ritchie *et al.* 1976; Garg *et al.* 2017; Quang *et al.* 2017). Change in the river turbidity concentration can occur because of the variation in the weather and climate patterns and also due to human activities near the bank of the river (Luis *et al.* 2019; Garg *et al.* 2020). pH is another critical water quality parameter very vital for the true sustainability of the aquatic and marine ecosystem. It is a non-bio-optical parameter (Sharma *et al.* 2019). The aquatic species may die if there is too much fluctuation occurring in the fluvial system. The optimum range of pH for freshwater aquatic animals lies between 6.5 and 9.0 (Wurts and Durborow 1992). DO is one of the most significant parameters of water quality for a sustainable aquatic ecosystem (Poole and Berman 2001; Null *et al.* 2017). The decreasing effect of the DO in the river shows negative consequences on aquatic ecosystems and biogeochemical processes (Middelburg and Levin 2009). DO has an inverse relationship with the temperature (Viswanathan *et al.* 2015; Null *et al.* 2017). TSS is another vital parameter that measures suspended sediments. Suspended sediments or solids are very problematic for the survival of aquatic species because they diminish the light, which is very much essential for aquatic life, and they also indicate eutrophication of the water bodies (Doxaran *et al.* 2002; Garg *et al.* 2017; Sebastiá-Frasquet *et al.* 2019).

The satellite imageries can estimate all the above-mentioned water quality parameters. The

satellite images consist of spectral bands, which can be helpful for the determination of these parameters (Pavelsky and Smith 2009; Khattab and Merkel 2014; El Din and Zhang 2017; Garg *et al.* 2017; Sharma *et al.* 2019).

The coronavirus disease 2019 (COVID-19) global pandemic is caused due to the novel coronavirus strain has been considered one of the most virulent diseases that affect human lives in around 210 countries (Chauhan and Singh 2020; Patel *et al.* 2020). To protect the population from this deadly disease, the government of each country had declared lockdown in a phased manner (Chauhan and Singh 2020). Similarly, the Indian government had also implemented a complete lockdown from midnight of 24th March 2020 (*The Lancet* 2020). Several studies have reported that due to the lockdown effect, the environmental conditions of major cities have been improved in terms of pruning in pollution of either air or water (Braga *et al.* 2020; Collivignarelli *et al.* 2020; Dantas *et al.* 2020; Lal *et al.* 2020; Muhammad *et al.* 2020; Otmani *et al.* 2020). The air and water quality of the major Indian cities had been improved because the lockdown brought about halting of work in factories, closure of the transport system and sealing of the commercial activities (CPCB 2020; Mahato *et al.* 2020). Due to this lockdown effect, the possible cleansing of the rivers occurred as a natural process (Shukla and Srivastava 2020), along with the cleansing of the river Ganga as well, which is one of the most polluted rivers (Hamner *et al.* 2013). The pollution level of river Ganga has been reduced, and it has become much cleaner now (Garg *et al.* 2020).

In this study, an attempt has been made for analysing several water-quality parameters such as temperature, turbidity, pH, DO and TSS for the river Ganga at different stretches. The temporal study of the Landsat-8 and Sentinel-2 data has been performed for the pre-lockdown, lockdown and post-lockdown time frame. Cloud-free satellite images have been considered for this study. For the processing of the image Google Earth Engine (GEE) platform has been used. GEE is a cloud-based technology operated by a massive number of servers worldwide, and it is freely available through the internet (Dong *et al.* 2016). Furthermore, as no field data were present for this time period, the results are represented in qualitative terms except for river temperature and normalised difference turbidity index (NDTI) values. Existing algorithms for calculating the river water temperature (Avdan and Jovanovska 2016) and NDTI (Lacaux *et al.* 2007) have been used in this analysis.

2. Materials and methods

2.1 *Study area*

The selected stretch area lies between Ghazipur and Mirzapur and is located in the northern part of India in southeastern Uttar Pradesh between the coordinates 82.52–83.60°E and 25.16–25.58°N (Yadav *et al.* 2020). This segment of the river comes under the geomorphological unit of central Ganga plains. In this region, the Ganga river plain is flat alluvial in nature, having a shallow depression and a small eastward gradient. The width of the river varies between 700 and 750 m in the study stretch, and the average height of this region is 76.19 m above the mean sea level (Rai *et al.* 2010; Pandey and Singh 2017). In this part, the summer season usually has a longer duration as compared to the winter season. The summer temperature varies between 32 and 47°C, whereas the winter temperature mostly hovers around the range of 5–15°C. The average annual precipitation in this region is 1110 mm (Das *et al.* 2020). Varanasi is a very famous city that lies in this region, and it is also called the spiritual capital of India. This city is also famous for silk products, ivory and sculptures (Garg *et al.* 2020). This study has been performed on the river stretch situated near the three cities that lie in the study area. The three stretches have been marked with red colour where the study was carried out as shown in figure 1. The red colour stretch for Mirzapur city lies between Ganjia (82.52°E, 25.16°N) and Kirtartara (82.59°E, 25.16°N). The colour stretch for the Varanasi region is situated between Ramna (83.02°E, 25.23°N) and Tatepur (83.06°E, 25.33°N). For the Ghazipur region, the stretch is located between Gorabazar (83.56°E, 25.55°N) and Jamalpur (83.60°E, 25.58°N).

2.2 *Conceptual framework of the water quality indices*

The term 'water-quality' was first coined by Horton, a US scientist, in 1965. This appeared as the most effective means to represent the overall
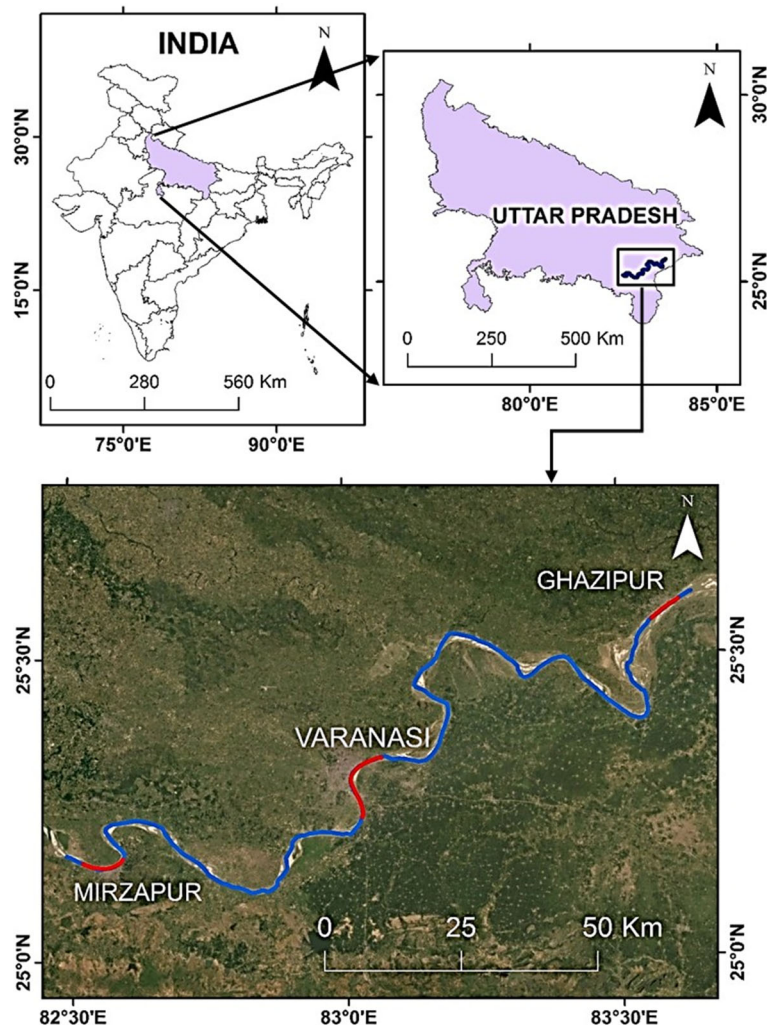
Figure 1. Geolocation map of the study area from Mirzapur to Ghazipur. The blue vector represents the entire river stretch. Red patches illustrate the river stretch considered for this analysis.

nature of water (Tyagi *et al.* 2013). Water quality has been defined in terms of the physical, chemical and biological parameters of water (Kachroud *et al.* 2019). Several agencies across the world such as the European Union, WHO (World Health Organisation) and some of the Indian agencies such as Central Pollution Control Board (CPCB) and ISSDW (Indian standard specification for drinking water) have prepared their standards regarding the acceptable limits of measured parameters for rating a sample as good/suitable for specific use (Sargaonkar and Deshpande 2003; Rout 2017). In this study, the water quality parameters such as temperature, turbidity, pH, DO and TSS have been considered. Among these parameters, some of them, such as pH and DO, have also been considered by CPCB for deriving the suitability of the water usage in different applications such as industrial

application, agricultural application and domestic household usages (Patel *et al.* 2020).

2.3 *Meteorological datasets*

The data used for meteorological parameters (air temperature and precipitation) have been derived from The Prediction of Worldwide Energy Resource (POWER) datasets of NASA. The meteorological data/parameters in POWER Release-8 are based on a single assimilation model from Goddard's Global Modelling and Assimilation Office. These datasets (interannual and daily timeseries format) are provided on a global grid having a spatial resolution of $0.5° \times 0.5°$ (Suarez *et al.* 2005). The POWER Data Access Viewer (DAV) is a web mapping application, and it contains geospatially enabled parameters. POWER

Table 1. *Time period for meteorological data.*

Time duration
28th January–12th February 2019
20th April–19th May 2019
1st November–15th November 2019
20th January–15th February 2020
15th April–5th May 2020
14th October–28th October 2020
18th April–24th May 2021

Table 2. *List of the satellite image datasets used.*

Satellite sensor	Date of the image acquisition
Landsat-8	11 February 2019
Landsat-8	18 May 2019
Landsat-8	14 November 2019
Landsat-8	14 February 2020
Landsat-8	4 May 2020
Landsat-8	27 October 2020
Landsat-8	7 May 2021
Landsat-8	23 May 2021
Sentinel-2	6 May 2019
Sentinel-2	10 February 2020
Sentinel-2	3 May 2020
Sentinel-2	27 October 2020
Sentinel-2	4 May 2021
Sentinel-2	23 May 2021

provides various texts', tabular, geospatial datasets and files that users can download and integrate into custom software and applications for further processing, analysis and visualisation. The time duration for which meteorological datasets have been prepared is presented in a tabular form in table 1.

2.4 *Satellite imagery datasets*

2.4.1 *Landsat-8 datasets*

Landsat-8 is the eighth member of the Landsat series, which is the joint mission of NASA and USGS. This satellite had been sent to the earth's orbit in February 2013, and the first image from this satellite was made available as of March 2013. This satellite consists of two independent working sensors: the operational land imager (OLI) and the other one is the thermal infrared (TIR). The OLI sensor has been used to gather information from the visible, near-infrared (NIR) and SWIR range of the EM spectrum. The TIR sensor is active on the thermal range (10.6–12.51 μm) of the EM spectrum. Landsat-8 satellite system consists of 11 bands of different wavelengths. There are two TIR bands in this satellite: band 10 (10.60–11.9 μm) and band 11 (11.50–12.51 μm). Band 8 of this satellite is panchromatic (PAN) band. Except for TIR and PAN band, all the bands have the spatial resolution of 30 m (Reuter *et al.* 2015). The TIR bands have a resolution of 100 m × 100 m, and the PAN bands have a resolution of 15 m × 15 m and the rest of the bands have a resolution of 30 m × 30 m. The TIR bands have been resampled to 30 m (Sekertekin and Bonafoni 2020). Both the TIR bands have excellent noise stability performance, but band 11 is affected more by stray values as compared to band 10 (Montanaro *et al.* 2014). In this analysis, band 10 has been used for the river temperature calculation. For the assessment of the

river temperature, 'Surface Reflectance Tier 1' datasets of the GEE domain have been used. These datasets are atmospherically corrected, and the correction has been carried out by using LaSRC (land surface reflectance code) algorithm (Vermote *et al.* 2016). The Landsat images used in this study have path 145/row 42 and 43.

2.4.2 *Sentinel-2 datasets*

Sentinel-2 (S2) satellite is a part of the Copernicus Sentinel 2 mission. S2A and S2B were commissioned in orbit in 2015 and 2017, respectively. The important usage for S2 images has been in studying lake ecology and water quality parameter estimation at a finer scale (Bresciani *et al.* 2018; Bhattacharjee *et al.* 2020). The temporal resolution of the S2A imager is 10 days, but it gets reduced to 5 days when both the sensors are operational. The spatial resolution of blue, green, red and NIR bands of the S2 satellite is 10 m as compared to the 30 m resolution of the same bands in the Landsat-8 satellite (Roy *et al.* 2014; Gorji *et al.* 2020). Level 2 products of S2 images are available in the GEE platform (Li *et al.* 2019), and these images have been used in this analysis.

The list of the satellite image datasets used from the two sensors (Landsat-8 and Sentinel-2) has been given in table 2.

2.5 *Methodology adopted for this analysis*

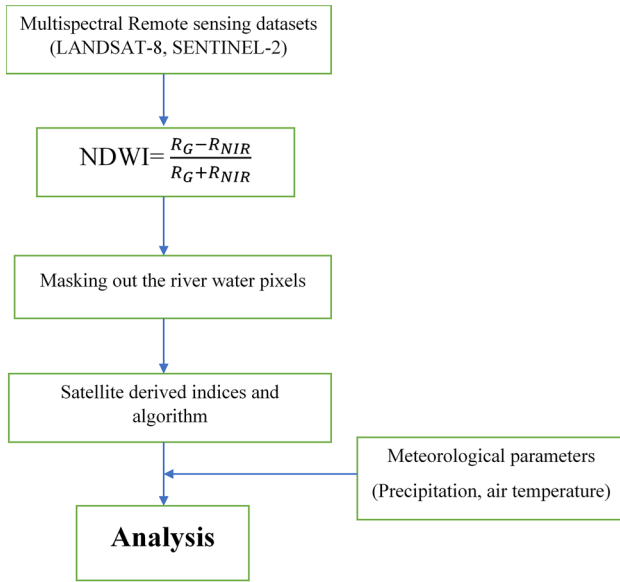Flowchart for the spatio-temporal analysis of the water quality parameters during the pre-lockdown,

Figure 2. Flowchart of the methodology for the analysis of the water quality parameter fluctuations.

lockdown and post-lockdown scenario has been drawn in figure 2. The water pixels have been delineated before applying the satellite-derived algorithms for estimating the water quality parameters.

2.5.1 *Masking out the water pixels*

Some of the water quality parameters such as temperature, turbidity, pH, DO and TSS have been analysed during the pre-lockdown, lockdown and post-lockdown time period. Sentinel-2 and Landsat-8 datasets have been used. Firstly, the water pixels have been identified for each of the satellite imagery used in this study. Delineation of the water pixels has been done by using normalised difference water index (NDWI). This technique was first proposed by McFeeters in 1996 (Garg *et al.* 2020). The NDWI formula has been given in equation (1):

$$\text{NDWI} = \frac{R_\text{G} - R_\text{NIR}}{R_\text{G} + R_\text{NIR}}. \tag{1}$$

In equation (1), the R_G and R_NIR represent the reflectance in green and NIR bands, respectively. The value of NDWI varies between -1 and $+1$. For theoretical purposes, if NDWI is more than zero for a particular pixel, then that pixel should be considered as a water pixel. But for practical purposes, NDWI values may vary for different

places. After the calculation of the NDWI value, the pixels containing water will get highlighted. These highlighted pixels have been masked out so that only water pixels remain for further analysis.

2.5.2 *Estimation of the river water temperature*

The water temperature has been calculated by the given formula (Avdan and Jovanovska 2016) as

$$T_\text{S} = \frac{\text{BT}}{\{1 + [(\lambda \text{BT}/\rho) \ln \varepsilon_\text{w}]\}} - 273.15, \tag{2}$$

where T_S is the calculated water temperature in °C, BT is the atmospherically corrected brightness temperature, and the value of BT has been calculated in Kelvin, λ is the peak emitted radiance, and its value has been considered as 10.895 μm. The ρ is a constant which has a value of 1.438×10^{-2} mK. The ε_w is the emissivity of the water, and the emissivity has been considered 0.988 (Ling *et al.* 2017) for this study. The water temperature has been calculated for the Landsat images only because the Sentinel-2 sensor does not contain the thermal bands, and the emissivity has been assumed to be a constant for the entire study stretch.

2.5.3 *Estimation of the river water turbidity*

The analysis of turbidity with the help of single-band algorithms sometimes procure results in underestimation and overestimation of sediment concentration in water (Kuhn *et al.* 2019; Pahlevan *et al.* 2019). Some extent of radiometric inconsistency can occur even in the temporal remote-sensing data of the same sensor, so relying on single-band information for turbidity calculation is not always a preferred choice (Pahlevan *et al.* 2019; Garg *et al.* 2020).

The turbidity has been calculated by using NDTI for this study. The NDTI formula uses red and green bands, and its values vary between -1 and $+1$ (Lacaux *et al.* 2007). The formula for NDTI is

$$\text{NDTI} = \frac{R_\text{R} - R_\text{G}}{R_\text{R} + R_\text{G}}, \tag{3}$$

where R_R and R_G are reflectances in the red band and green band, respectively. For low, moderate

and high turbidity values, average and SD (standard deviation) were calculated as follows:

Low turbidity = Average turbidity − SD,
Moderate turbidity = Average turbidity + SD,
High turbidity = more than moderate turbidity.

For pure water, it generally has been found that reflectance has been more in the green band as compared to the red band, but for the turbid water, the red band has more reflectance in comparison with the green band (Ritchie *et al.* 1976; Moore 1980; Gholizadeh *et al.* 2016; Garg *et al.* 2020). When the value of turbidity becomes high, then the NDTI value also increases and vice versa.

2.5.4 *Estimation of the pH, DO and TSS*

Water quality parameters (pH, DO and TSS) have been calculated by using both the Landsat and Sentinel-2 satellite imageries. Due to the lockdown, sampling for the water quality parameters has not been possible. The value of the water quality parameters has been derived from satellite-based indices. The following indices have been calculated with the help of Landsat imageries.

The pH has been determined by using the following formula (Sharma *et al.* 2019):

$$\mathrm{pH} = 8.35 - 2\left(\frac{R_{\mathrm{NIR}}}{R_{\mathrm{Blue}}}\right) + 18.4 R_{\mathrm{NIR}}. \quad (4)$$

The DO has been computed by using the following formula (Sharma *et al.* 2019):

$$\mathrm{DO} = 8.2 - 0.15\left(\frac{R_{\mathrm{Blue}}}{R_{\mathrm{NIR}}}\right) - 0.32\left(\frac{R_{\mathrm{Green}}}{R_{\mathrm{NIR}}}\right). \quad (5)$$

The TSS has been calculated (El Din and Zhang 2017) as follows:

$$\mathrm{TSS} = 13.068\left(\frac{R_{\mathrm{Coastal\,Blue}}}{R_{\mathrm{Red}}}\right) + 70.19\left(\frac{R_{\mathrm{Red}}}{R_{\mathrm{Blue}}}\right) - 66.034. \quad (6)$$

The following indices have been enumerated using Sentinel-2 imageries.

The pH has been calculated by (Torres-Bejarano *et al.* 2020)

$$\mathrm{pH} = 4.925 - 0.03739\left(\frac{R_{\mathrm{Red\,Edge\,2}}}{R_{\mathrm{Red}} - R_{\mathrm{NIR}}}\right) + 2.478\left(\frac{R_{\mathrm{Red\,Edge\,3}}}{R_{\mathrm{Red\,Edge\,2}}}\right). \quad (7)$$

The DO have been determined (Torres-Bejarano *et al.* 2020) as follows:

$$\mathrm{DO} = -1.687 + 13.65\left(\frac{R_{\mathrm{Red\,Edge\,1}}}{R_{\mathrm{Red}} + R_{\mathrm{Narrow\,NIR}}}\right) - 0.3714\left(\frac{R_{\mathrm{Red}}}{R_{\mathrm{Red\,Edge\,3}} - R_{\mathrm{NIR}}}\right). \quad (8)$$

The TSS has been quantified by using the formula (Ouma *et al.* 2020):

$$\mathrm{TSS} = 46505.5\left(R_{\mathrm{Red}} + \frac{R_{\mathrm{NIR}}}{R_{\mathrm{Red}}}\right)^2 - 41386.5\left(R_{\mathrm{Red}} + \frac{R_{\mathrm{NIR}}}{R_{\mathrm{Red}}}\right) + 18442. \quad (9)$$

3. Results

3.1 *Statistical representation of river temperature and NDTI values*

The result has been presented in the form of a box plot for river temperature and NDTI during the time period of pre-lockdown, lockdown and post-lockdown. For the temperature representation, February 2019 and 2020, May 2019 and 2020, November 2019 and October 2020 have been considered. Different months (October and November) have been chosen for this study because of the cloud cover issue associated with Landsat-8 imageries. River temperature in the Ghazipur region during February 2019 lies between 18 and 21°C, with a majority of the values situated between 19 and 20°C. However, for the period of February 2020, the temperature is situated between 19 and 21°C with most of the values falling within 20–20.5°C. Amid May 2019, the temperature lies in the range of 27.5–29°C, and for May 2020 (during lockdown), the temperature hovers between 25.5 and 26.5°C. November is relatively colder than October, so November 2019 (22.2–23.8°C) has a lower temperature as compared to October 2020 (24.4–26°C). For the Varanasi region, the temperature range for February 2019 (19–20.8°C) is lower as compared to February 2020 (22–23°C). In the season of May 2019, the temperature hovers from 28.4 to 31°C, and during May 2020 (lockdown period), the temperature lies in the range of 26–27°C. The month of November is relatively colder as compared to October, so November 2019 had a temperature range between

24 and 24.8°C, and October 2020 has a temperature range between 26 and 27°C. The Mirzapur region also shows a similar trend to that of Varanasi and Ghazipur. The significant temperature range of February 2019 (19–20°C) is lower than that of February 2020 (20–21°C). The temperature range of May 2019 (28–30.4°C) is more as compared to the lockdown period during May 2020 (25–27°C). The November 2019 temperature range (22.6–24°C) is lower than that of October 2020 (25–26°C) (figure 3a).

The NDTI values have been calculated for the time period of May 2019, February 2020, May 2020 and October 2020 using Sentinel-2 datasets. The NDTI trend for all three stretches shows a similar pattern that NDTI shows a slight downward trend in February 2020 as compared to May 2019. Then in May 2020 (during lockdown), the NDTI shows a significant decrease as compared to February 2020 (pre-lockdown time). Again, in October 2020, the NDTI parameter indicates an upward trend. During the period of February 2019, the NDTI values for all three stretches lie primarily within the range of 0.03–0.1. For February 2020, the Varanasi region indicates the highest NDTI range from 0.025 to 0.06 among all the stretches. The Mirzapur stretch exhibits a higher NDTI range (0.025–0.05) compared to the Ghazipur region (0.02–0.045). During the time of lockdown (May 2020), the NDTI range for Varanasi stretch hovers between −0.25 and −0.15. In the same time period, Ghazipur and Mirzapur indicate NDTI range between −0.24 to −0.1 and −0.23 to −0.12, respectively. For the period of October 2020, the NDTI range of Ghazipur, Varanasi, and Mirzapur are −0.25 to −0.05, −0.23 to −0.08 and −0.2 to −0.049, respectively (figure 3b).

During the period of the second lockdown, the river temperature shows a steady increase for the region of Ghazipur, Varanasi and Mirzapur. In early May 2020, the river temperature in Ghazipur river stretch ranges between 25.5 and 26.5°C. In early May 2021, at the same place, the temperature varies between 27 and 28.8°C. In late May 2021, the temperature further increased from 28.7 to 31.5°C. In the Varanasi as well as Mirzapur river stretch also the same pattern has been followed. In comparison with early May 2020, early May 2021 shows an increment of approximately 2°C rise in the median river temperature for the Varanasi stretch. The median temperature rises by 4°C in later May 2021 as compared to early May 2021. The river

temperature value for the Mirzapur stretch ranges from 27.5 to 30°C in early May 2021 as compared to the 25 to 26.8°C in early May 2020. The river temperature further increases in the later period of May 2021. In that period, the river temperature ranges between 29.5 and 32°C (figure 3c).

The turbidity value also increases in the later part of May 2021 as compared to early May 2021 for the considered stretches. For all the considered stretches, the river turbidity shows a high value in early May 2021 period as compared to early May 2020. For the Ghazipur stretch, the median NDTI increases by 0.22 in early May 2021 as compared to early May 2020. In later May 2021, the median NDTI value further increased by 0.02 in comparison with early May 2021. In the Varanasi stretch, in early May 2020, the NDTI ranges between −0.25 and −0.15, and in early May 2021, the NDTI value hovers between 0.02 and 0.08. The NDTI shows a slight increase in the later May 2021 period when it ranges between 0.04 and 0.10. For the Mirzapur stretch, the NDTI depicts an almost similar range in the early and later period of May 2021. For early May 2021, the NDTI ranges between 0.02 and 0.08, and for the later May 2021 period, it ranges between 0.03 and 0.09. In early May 2020, the NDTI value was considerably less, and it varies between −0.23 and −0.12 (figure 3d).

3.2 *Relation between river temperature and water quality parameters for Varanasi stretch*

The correlation graphs have been plotted for the Varanasi region for the period of May 2019 (a year before the lockdown time period) and May 2020 (lockdown time period). The river temperature decreases during the lockdown.

The clustering of the pH values have occurred between 7.4 and 7.8 during the lockdown, but in the previous year (May 2019), the pH clustering occurs at two places, i.e., between 6.3 and 6.5 and nearby 8.0. Similarly, the DO also shows the two clusters for the pre-lockdown time period (May 2019) and almost a single cluster during the lockdown time period (May 2020). NDTI has formed the cluster within the range of −0.25 to −0.17 for the lockdown period. For May 2019, the NDTI has been clustered between 0.05 and 0.07 (figure 4).
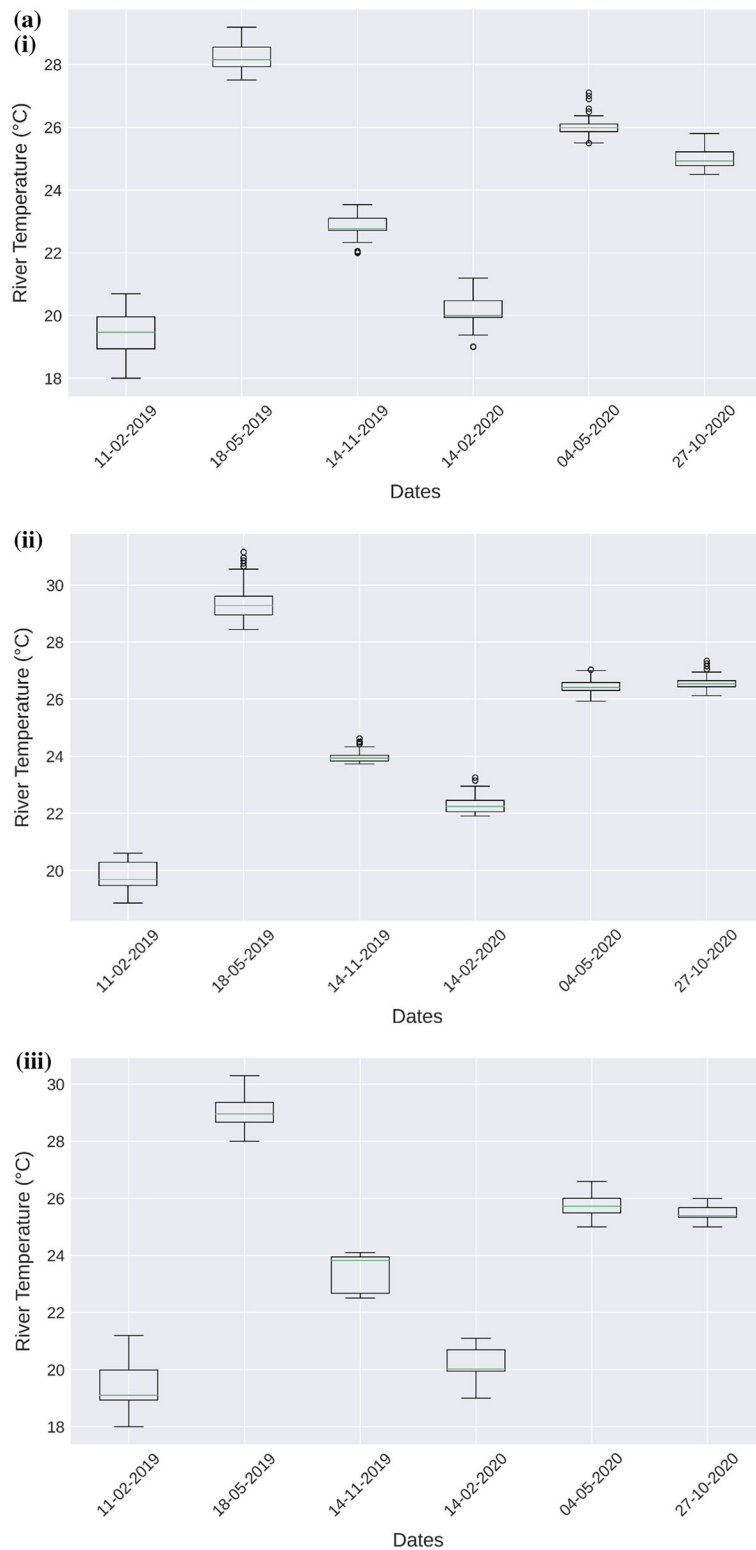
Figure 3. (**a**) Box-plot representation of the river temperature (°C) using Landsat-8 datasets for the stretch of (i) Ghazipur, (ii) Varanasi and (iii) Mirzapur. (**b**) Box-plot representation of the NDTI values using Sentinel-2 datasets for the stretch of (i) Ghazipur, (ii) Varanasi and (iii) Mirzapur. (**c**) Box-plot representation of the river temperature (°C) for the analysis of the second wave COVID-19 lockdown effect using Landsat-8 datasets for the stretch of (i) Ghazipur, (ii) Varanasi and (iii) Mirzapur. (**d**) Box-plot representation of the NDTI values for the analysis of the second wave COVID-19 lockdown effect using Sentinel-2 datasets for the stretch of (i) Ghazipur, (ii) Varanasi and (iii) Mirzapur.

(b)
(i)

(ii)

(iii)

Figure 3. (*Continued.*)

(c)
(i)

(ii)

(iii)
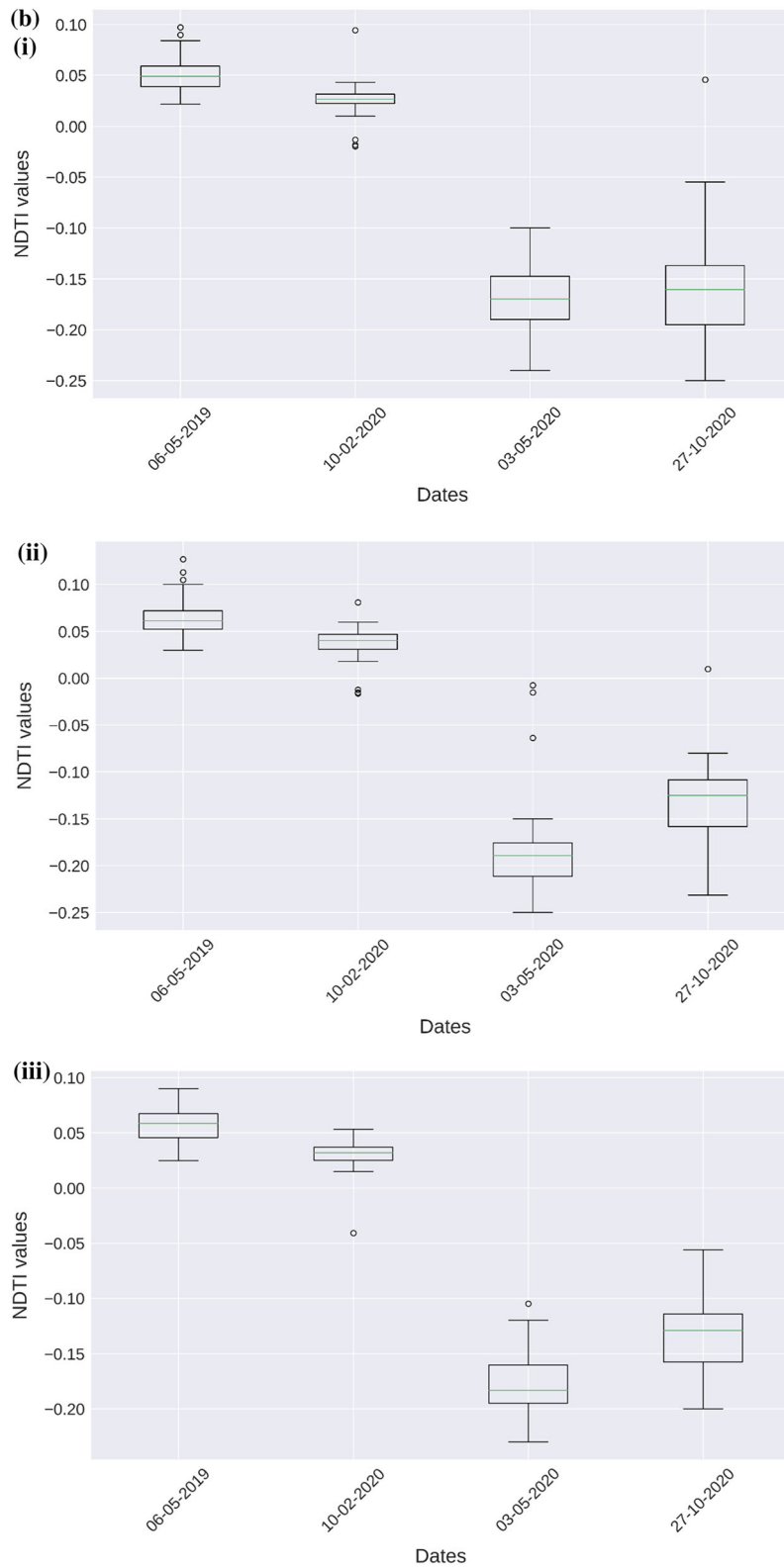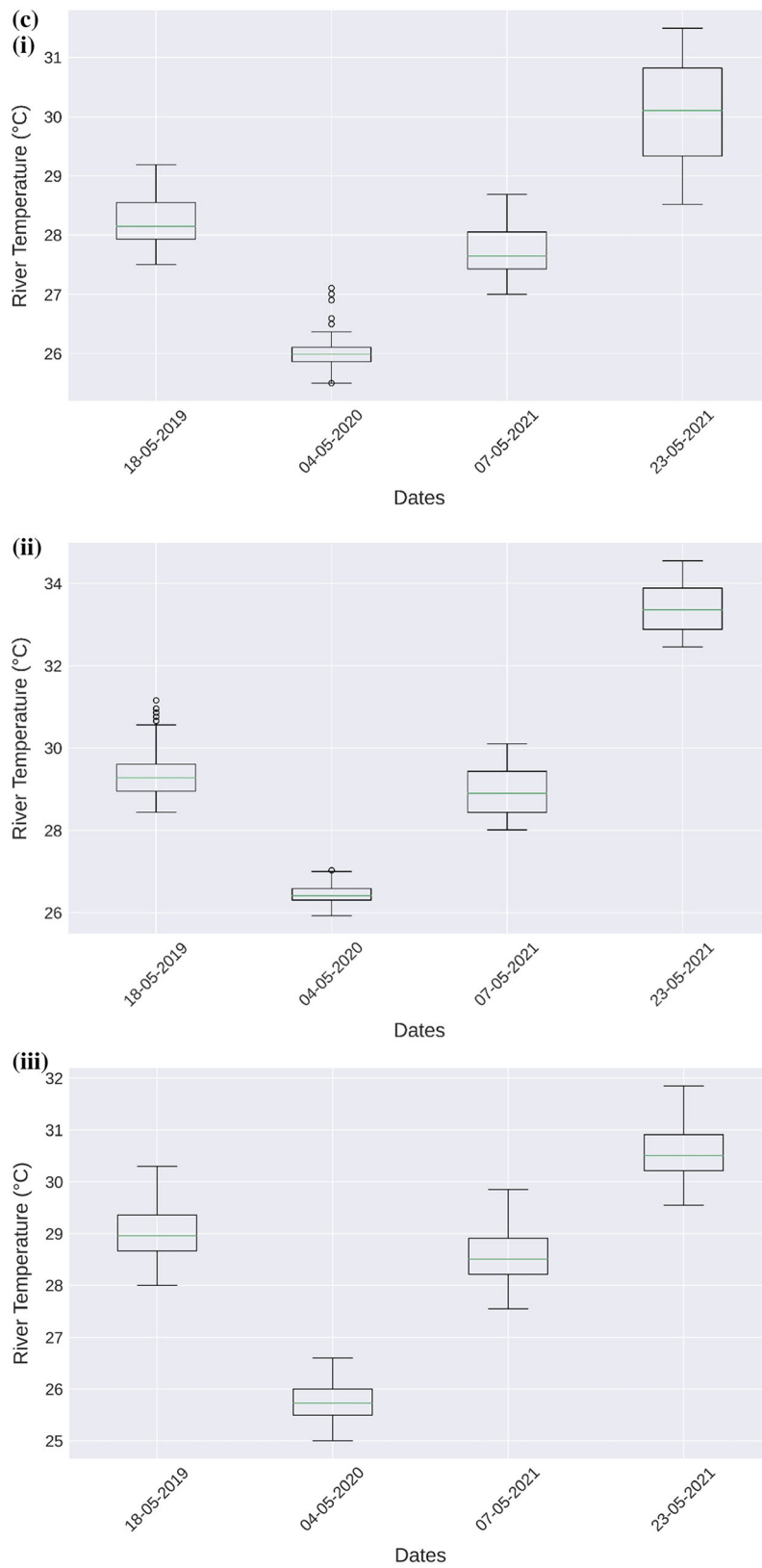
Figure 3. (*Continued.*)
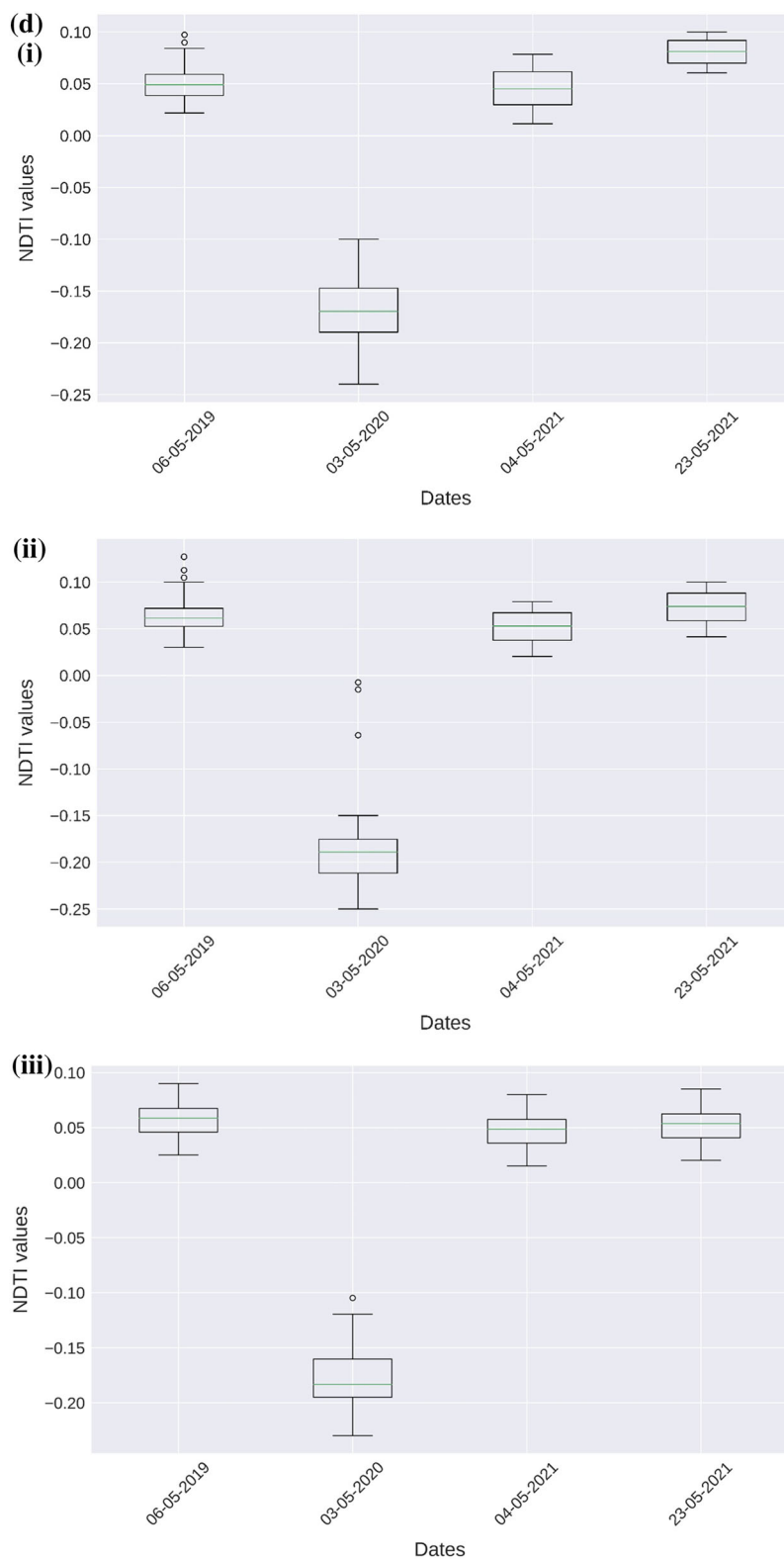
Figure 3. (*Continued.*)
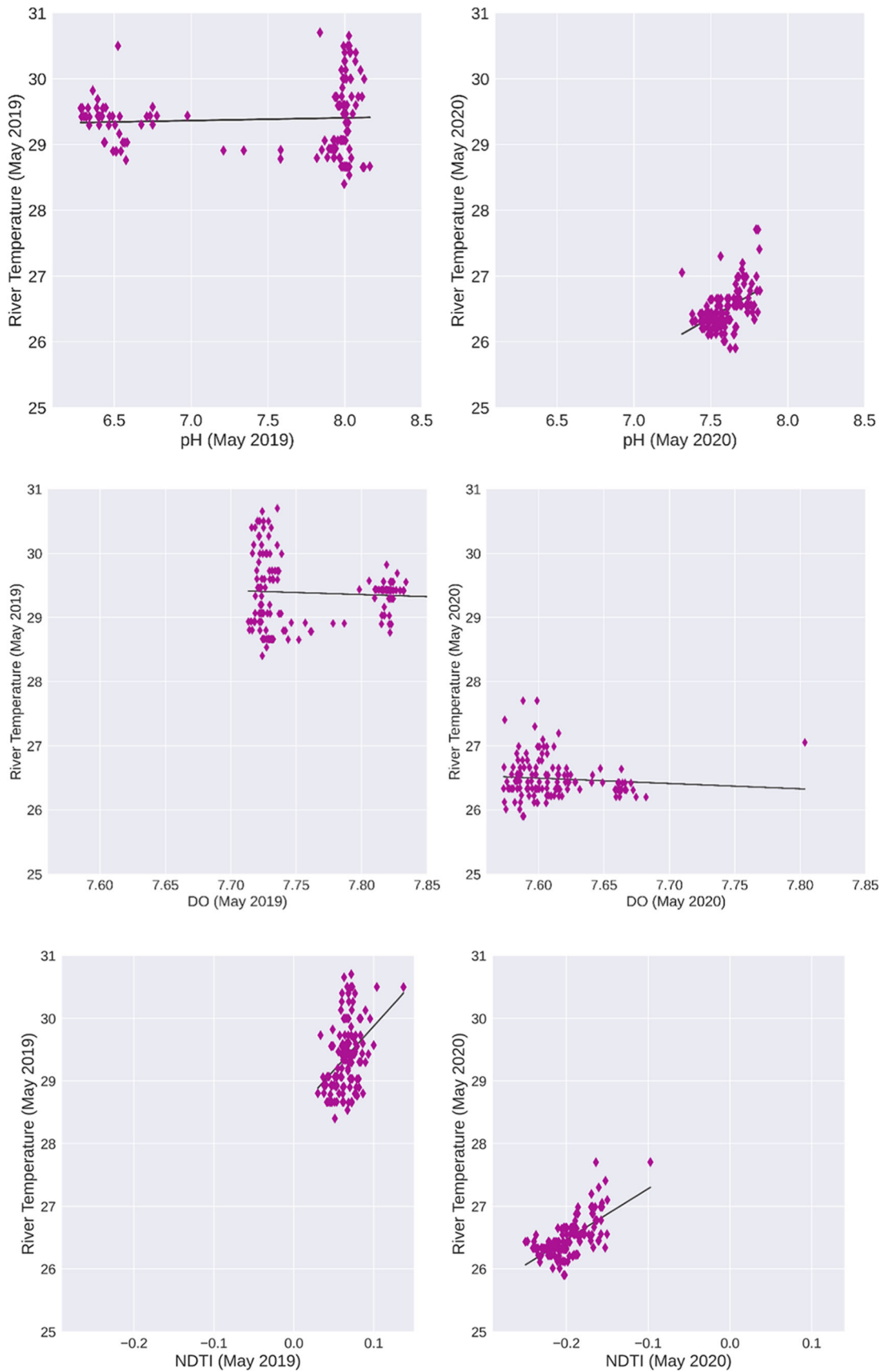
Figure 4. Correlation plot between river temperature (°C) and water quality parameter(s) using Landsat-8 datasets for the Varanasi stretch during May 2019 and May 2020.

3.3 *Map representation*

3.3.1 *Qualitative representation of the water quality parameters at different stretches*

The water quality parameters have been represented in qualitative terms for Ghazipur, Varanasi and Mirzapur stretch. For this representation, the difference maps have been generated using Sentinel-2 imageries. The difference map (May 2020–May 2019) of pH shows high and very high differences for all the considered stretches. The difference map of 'May 2020–February 2020' for Ghazipur and Varanasi stretch depicts low and medium fluctuation for pH, but the Mirzapur difference map for the same timestamp has some changes as well. For the difference map of 'May 2020–October 2020', the fluctuation of pH remains mostly low and very low for the Varanasi stretch. Mirzapur stretch also follows more or less the same pattern except for some places where pH fluctuation becomes high. The Ghazipur stretch during the same timestamp mostly has a medium and low change of pH, and sporadically high pH change has also been noticed (figure 5a).

The difference map (May 2020–May 2019) of DO shows high and very high fluctuation for all the stretches. The DO difference map of 'May 2020–February 2020' shows mostly medium and low alteration for the Varanasi stretch and mostly medium variation for the Mirzapur stretch. The Ghazipur stretch also has mostly medium variation, but there has been very low and high variation at some patches. From the difference map of 'May 2020–Oct 2020', it can be depicted that for the Varanasi and the Mirzapur stretch, DO fluctuation mostly remain low, and for the Ghazipur stretch, the alteration in the DO is very low (figure 5b).

The difference map (May 2020–May 2019) of TSS shows high and very high fluctuation for the Varanasi stretch. Fluctuation becomes mostly very high for the Ghazipur and the Mirzapur stretch. The TSS difference map of 'May 2020–February 2020' show mostly medium variation for the Varanasi stretch. Even for the Ghazipur and the Mirzapur stretch, mostly medium variation persist, but at some patches, high and very high variation also show their presence. The difference map 'May 2020–Oct 2020' of TSS shows mostly low and very low alteration for all considered study stretches (figure 5c).

Qualitative analysis has been presented only because the field sampling for the water quality parameters has not been possible due to the lockdown scenario over the entire country. Therefore, the validation procedure cannot be performed. Therefore, only qualitative work has been conducted for this study.

3.3.2 *Changing patterns of the river temperature and NDTI values for Varanasi stretch*

The temperature map has depicted the change in the river thermal pattern for the Varanasi stretch. For the time period of February 2019 and February 2020, the river temperature shows an upward trend for the considered stretch for the timestamp of February 2020. During the lockdown time (May 2020), the river temperature portrays a considerable decline compared to May 2019 temperature. The temperature mostly lies between 28.5 and 29.5°C during May 2019, but in May 2020, temperature mostly ranges between 26.5 and 27°C. November usually becomes colder as compared to October in this part of the world, so the temperature of November 2019 (mostly ranges between 23.8 and 24°C) is less than that of October 2020 (mostly ranges between 26.2 and 26.8°C) (figure 6).

The NDTI values have been represented for the period of May 2019 (before the lockdown period), February 2020 (before the lockdown period), May 2020 (the lockdown period) and October 2020 (the post-lockdown period) for the Varanasi stretch. During May 2019, NDTI primarily lies in the range of 0.05–0.07. In February 2020, NDTI decreased as compared to May 2019. During lockdown time (May 2020) NDTI value reduced significantly, and it mainly lies in the range of −0.21 to −0.17. In the post-lockdown period (October 2020), NDTI showed an upward trend as compared to the lockdown period (figure 7).

The two dates have been considered for May 2021. The river temperature lies mainly in a similar range for early May 2021 and May 2019. In May 2019, the temperature ranged between 28.5 and 30.7°C. In early 2021, the range of the temperature is from 28 to 30°C. In the later part of May 2021, the river temperature hovers between 32.5 and 34.5°C. The later May 2021 period has the highest temperature among all the considered time frames (figure 8).
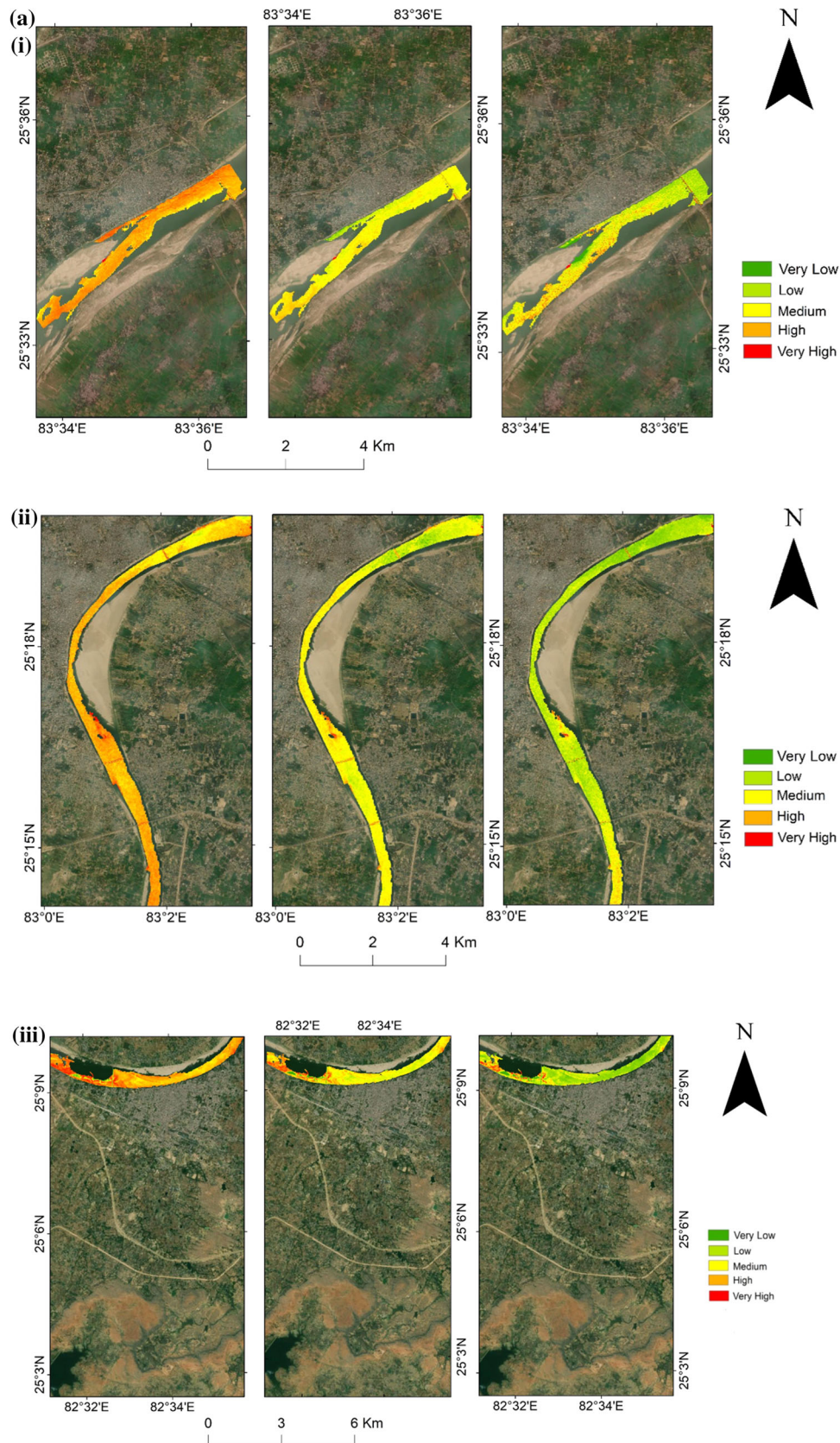
Figure 5. (**a**) Qualitative difference maps [(May 2020–May 2019), (May 2020–February 2020), (May 2020–October 2020)] of pH using Sentinel-2 datasets for the stretch of (i) Ghazipur, (ii) Varanasi and (iii) Mirzapur. (**b**) Qualitative difference maps [(May 2020–May 2019), (May 2020–February 2020), (May 2020–October 2020)] of DO using Sentinel-2 datasets for th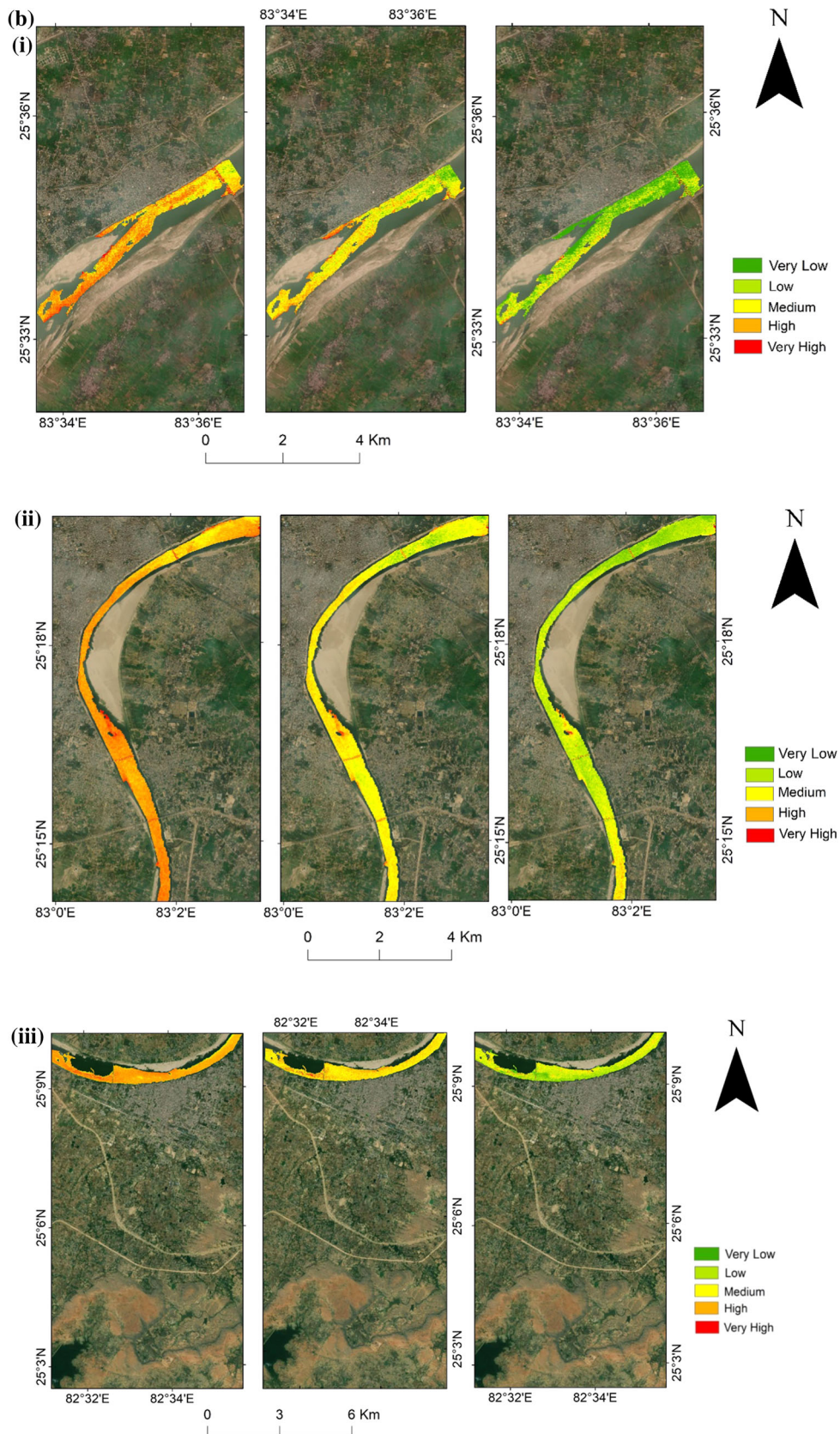e stretch of (i) Ghazipur, (ii) Varanasi and (iii) Mirzapur. (**c**) Qualitative difference maps [(May 2020–May 2019), (May 2020–February 2020), (May 2020–October 2020)] of TSS using Sentinel-2 datasets for the stretch of (i) Ghazipur, (ii) Varanasi and (iii) Mirzapur.
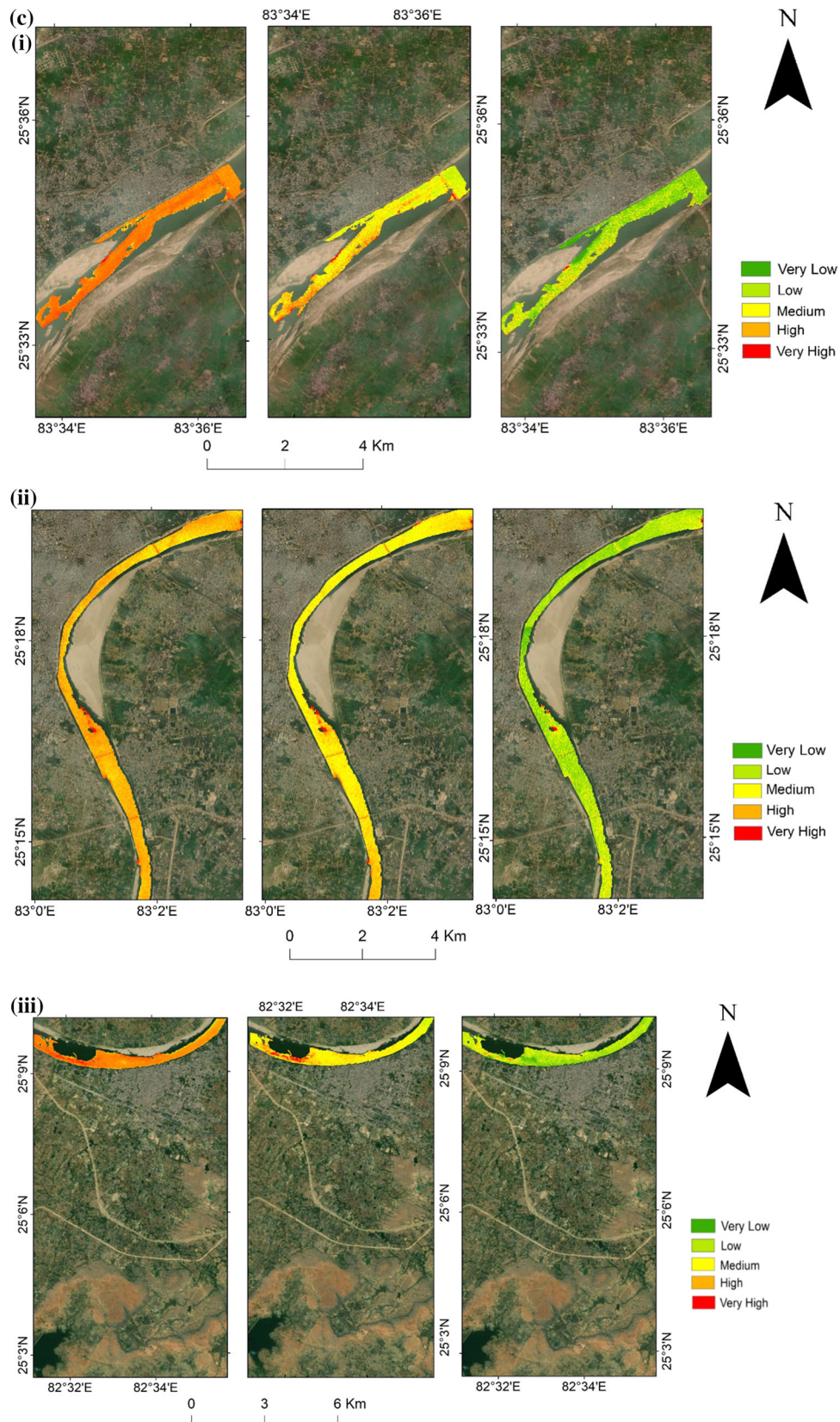
Figure 5. (*Continued.*)

Figure 5. (*Continued.*)

The NDTI value for the time period of May 2019 and May 2021 lies in the range of 0.03–0.10. The NDTI for early May 2021 lies between 0.03 and 0.08. The range for the period of May 2019 and late May 2021 was almost similar. The NDTI value has been considerably low in May 2020, and it hovers between −0.25 and −0.15 (figure 9).

4. Discussion

4.1 *Analysis of the spatio-temporal change in river temperature and NDTI*

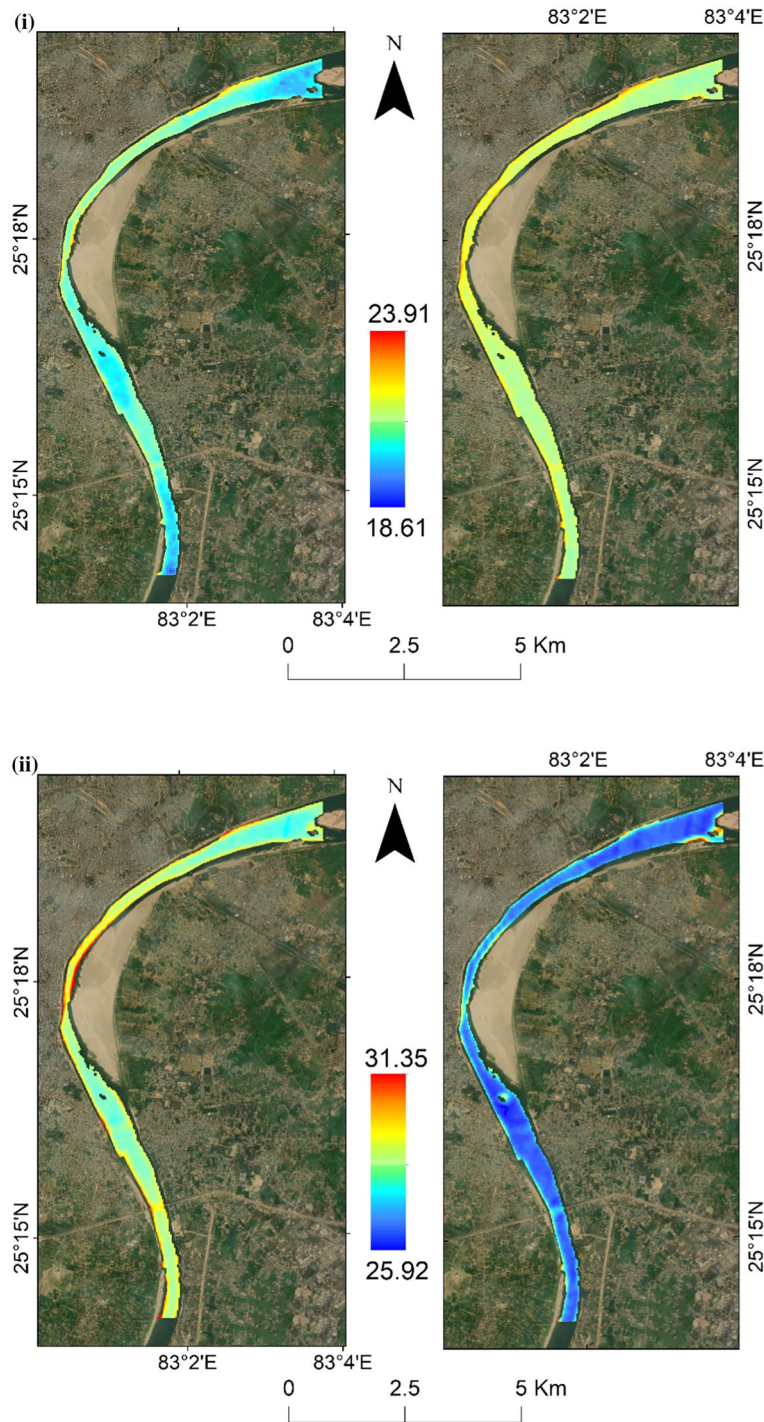The quantitative analysis has been carried out for the river temperature parameter for the considered

Figure 6. River temperature (°C) variation for the Varanasi stretch using Landsat-8 datasets during the time period of (i) February 2019 and February 2020, (ii) May 2019 and May 2020 and (iii) November 2019 and October 2020.
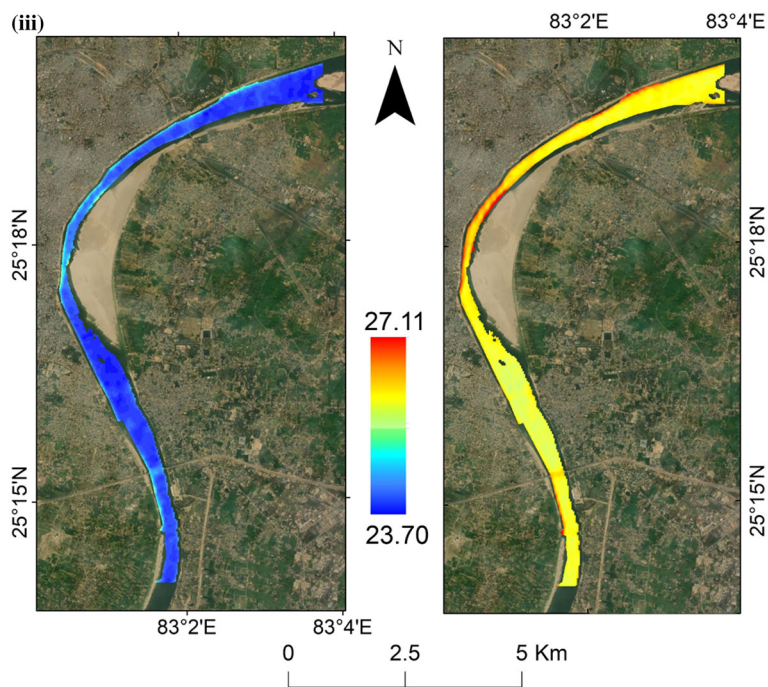
Figure 6. (*Continued.*)

stretches and for the stipulated period. The temperature estimation formula is a well-known formula and has been already applied by several researchers across the globe, including India (Avdan and Jovanovska 2016; Orhan and Yakar 2016; George *et al.* 2017; Barbieri *et al.* 2018; Rongali *et al.* 2018). The river temperature is one of the essential parameters for the sustainable development of the aquatic ecosystem (Wawrzyniak *et al.* 2012; Ling *et al.* 2017). Fishes are one of the important pillars of the aquatic ecosystem because they act as contributors of nutrients to this ecosystem (Layman *et al.* 2013). At Varanasi and nearby (Ghazipur and Mirzapur) stretches, 82 different varieties of fish species were recorded in the river Ganga (Dwivedi *et al.* 2016). Change in the river temperature can affect the fish network structure in the river (Brown and Krygier 1970).

For all of the considered stretches, the temperature has been more in February 2020 as compared to February 2019, and global warming can be one of the causes for this increase in the river temperature (Wawrzyniak *et al.* 2016). The river temperature shows a declining trend in the lockdown period (May 2020) in comparison with that of May 2019. The decrease in the river temperature can be attributed to the fact that the river temperature reduces because of the dwindling effect of air temperature. The air temperature has a direct relationship with the river water temperature (Webb 1996; Poirel *et al.* 2009). The air temperature gets reduced because the lockdown has forced to shut down the industries, due to which the carbon emissions get depleted. Concentrations of PM_{10} and $PM_{2.5}$ have witnessed the maximum reduction (Mahato *et al.* 2020). The region of Mirzapur and Varanasi is an industrial belt. Mirzapur is rich in metalware and utensil manufacturing industries (Sharma *et al.* 1992). In Varanasi and the nearby regions, several industries such as textile, chemical and metal processing are situated (Rai and Tripathi 2008; Rai *et al.* 2010). Heavy metals such as Zn, Cu, Cd, Pb, Cr and Ni have been found in the river among these stretches (Sharma *et al.* 1992; Rai *et al.* 2010). These heavy metals are very harmful to the aquatic ecosystem (Baby *et al.* 2010). Heavy metals can increase the electrical conductivity of the river, which can enhance the river temperature (Kefford 1998). However during lockdown, the industries were closed, so there has been less discharge of heavy metals into the river, which could also be another factor for low river temperature during the lockdown period. The strict lockdown had been implemented in India from the last week of March 2020 to July 2020 (Saravanan 2020). Several industries in this region still have not become fully functional even after July 2020. The river thermal pattern during post-lockdown (October 2020) has shown an
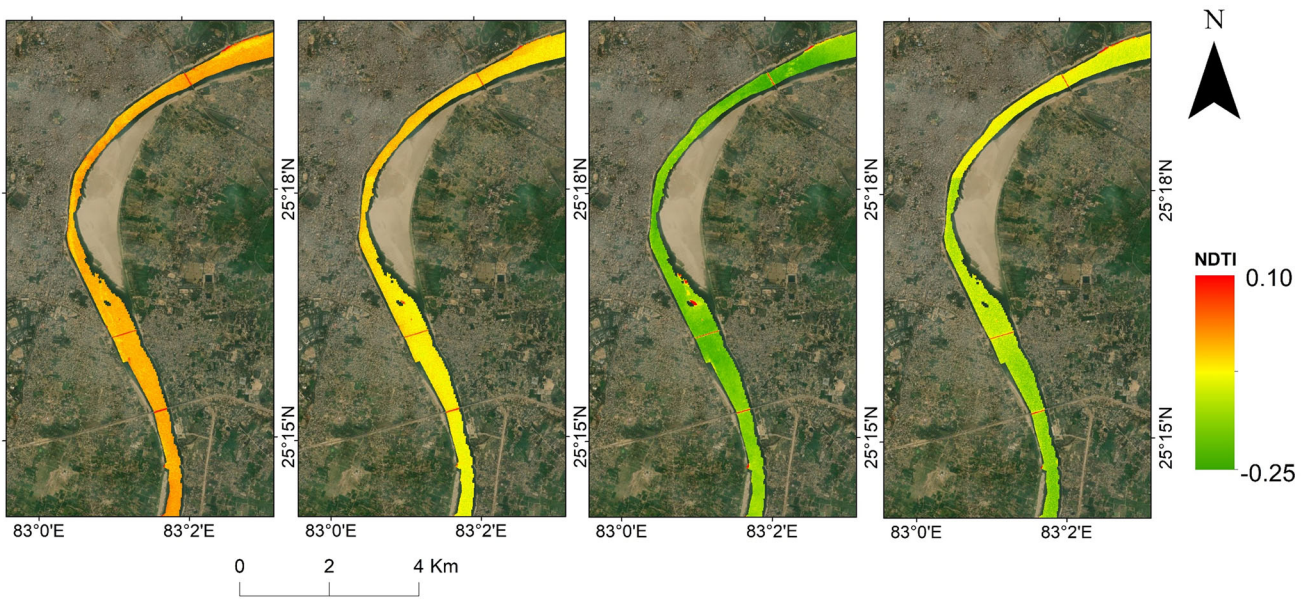
Figure 7. NDTI values for the Varanasi stretch using Sentinel-2 datasets for the time period (May 2019, February 2020, May 2020 and October 2020).
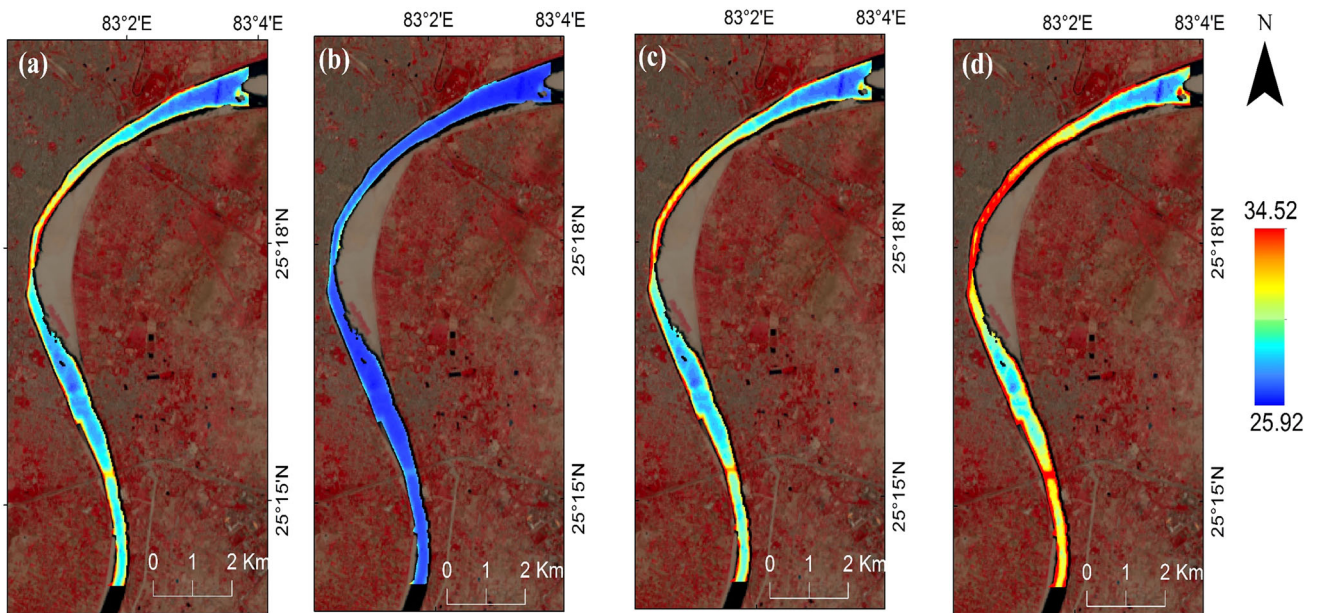

Figure 8. River temperature (°C) variation for the Varanasi stretch using Landsat-8 datasets during the time period of (**a**) May 2019, (**b**) May 2020 and (**c**) and (**d**) May 2021.

increasing trend as compared to November 2019. This is a natural phenomenon as the air temperature in the month of October is more as compared to November, and the river temperature also follows the same pattern.

In the Indian subcontinent region, it has been already estimated that NDTI varies from −0.2 to 0.0 in the case of clear water and from 0.0 to 0.2 in the case of moderately turbid water. For highly turbid water, NDTI values go beyond 0.25 (Subramaniam and Saxena 2011). During the pre-lockdown time (May 2019 and February 2020), the considered stretches have been moderately turbid. The NDTI value has been highest for the Varanasi stretch. It can be attributed to the fact that it is the most populated city in this entire stretch. The anthropogenic activities near the riverbank of Varanasi are also high compared to the other two
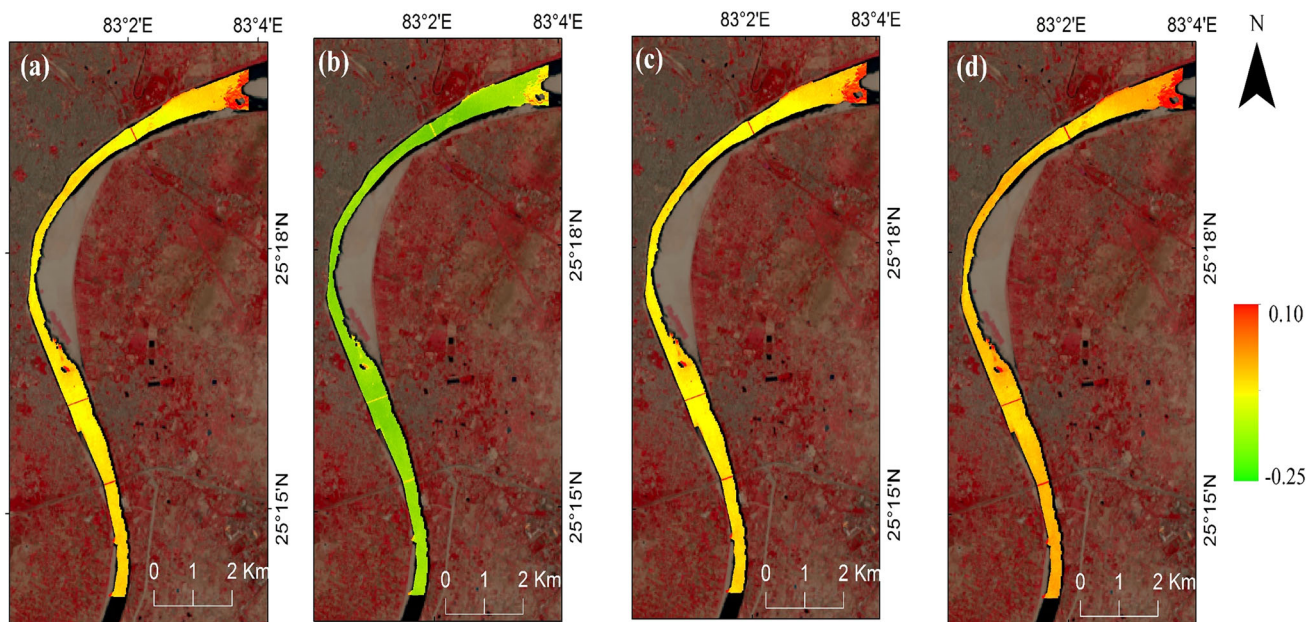
Figure 9. NDTI values for the Varanasi stretch using Sentinel-2 datasets for the time period of (**a**) May 2019, (**b**) May 2020 and (**c**) and (**d**) May 2021.

cities (Mirzapur and Ghazipur). The industrial and domestic waste discharge can also inflate the turbidity of the river. The Assi and Varuna rivers have a confluence with river Ganga in the Varanasi stretch. These two rivers increase the microbial load in this stretch (Trombadore *et al.* 2020), so this can also act as an additional factor for more turbidity (Tornevi *et al.* 2014) in the Varanasi stretch, as compared to other stretches. Discharge of the heavy metals from the industries in this entire study stretch is also a factor for the turbid river water in this region (Nasrabadi *et al.* 2016). Turbidity is a significant optical property of water that diminishes the energy required for aquatic growth. An increase in turbidity can hinder the growth of aquatic flora and fauna. Photosynthesis will be reduced, and that, in turn, will deplete the productivity of the aquatic flora system. Turbidity in the river can also cause a disruption of the mating system among fishes (Järvenpää and Lindström 2004). This region is the home of nearly 80 different fishing species (Dwivedi *et al.* 2016), so an increase in turbidity can disrupt the fish network structure of this region. This can eventually collapse the aquatic environment of the study stretch under consideration. The effect of lockdown has become a blessing in disguise for aquatic ecosystems. Due to this, the anthropogenic activities become very minimal on the river bank, and domestic waste discharge in the river has also drastically reduced. The majority of the industries

remained closed during the lockdown and very minimal amount of industrial waste was discarded into the river. These kinds of unusual scenarios decrease river turbidity (May 2020), which in turn immensely enhance the aquatic ecosystem of this region. Even during the post-lockdown period (October 2020), most of the industries remained closed, and significantly fewer anthropogenic activities took place, therefore river Ganga was non-turbid. The additional meteorological effects (rainfall and air temperature) have also been analysed. The average precipitation and average air temperature of the stretch have been considered for this study. There is not much variation in the meteorological parameters for 2019 and 2020. During April–May 2020, a considerable amount of rainfall (>10 mm) occurred on one day, however, for other days rainfall was less than 4 mm (figure 10).

4.2 *Analysis of the qualitative difference maps of the water quality parameters*

Qualitative maps for the water quality parameters (pH, DO and TSS) have been prepared. The lockdown period (May 2020) has been considered the base time period. In comparison with that, the change in scenario for water quality parameters over the study stretch has been analysed. For the pH, it can be seen that the difference map (May

2020–May 2019) shows a high fluctuation of the pH for all the study stretch. This can be because, in May 2019, everything was normal; the industries were running at their full capacity, wherein industrial waste discharges, anthropogenic activities along with domestic wastes in the river Ganga made the river acidic. Due to lockdown, all these activities came to a grinding halt partially or entirely, so there was a stark change observed between the difference map (May 2020–May 2019) concerning pH. Similarly it can be said for the DO difference map (May 2020–May 2019) also. During normal times due to the excessive waste discharge into the river and anthropogenic activities alarmingly diminish the DO. The variation in the pH for the
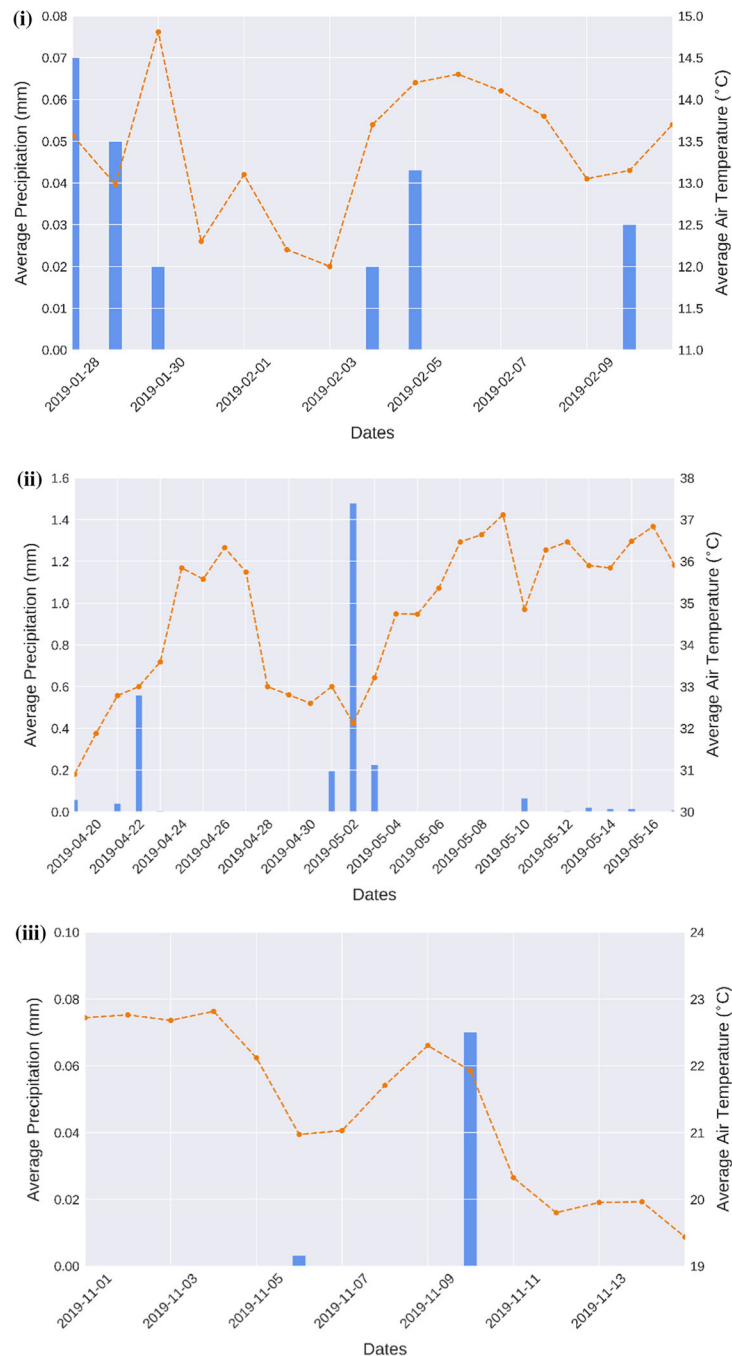

Figure 10. Graphical representation of the meteorological parameters (air temperature and rainfall) for the time period (i) 28th January–12th February 2019, (ii) 20th April–19th May 2019, (iii) 1st November–15th November 2019, (iv) 20th January–15th February 2020, (v) 15th April–5th May 2020, (vi) 14th October–28th October 2020 and (vii) 18th April–24th May 2021. Note: Air temperature has been represented in the form of dots and dotted lines. Rainfall has been denoted in the form of bar diagrams.
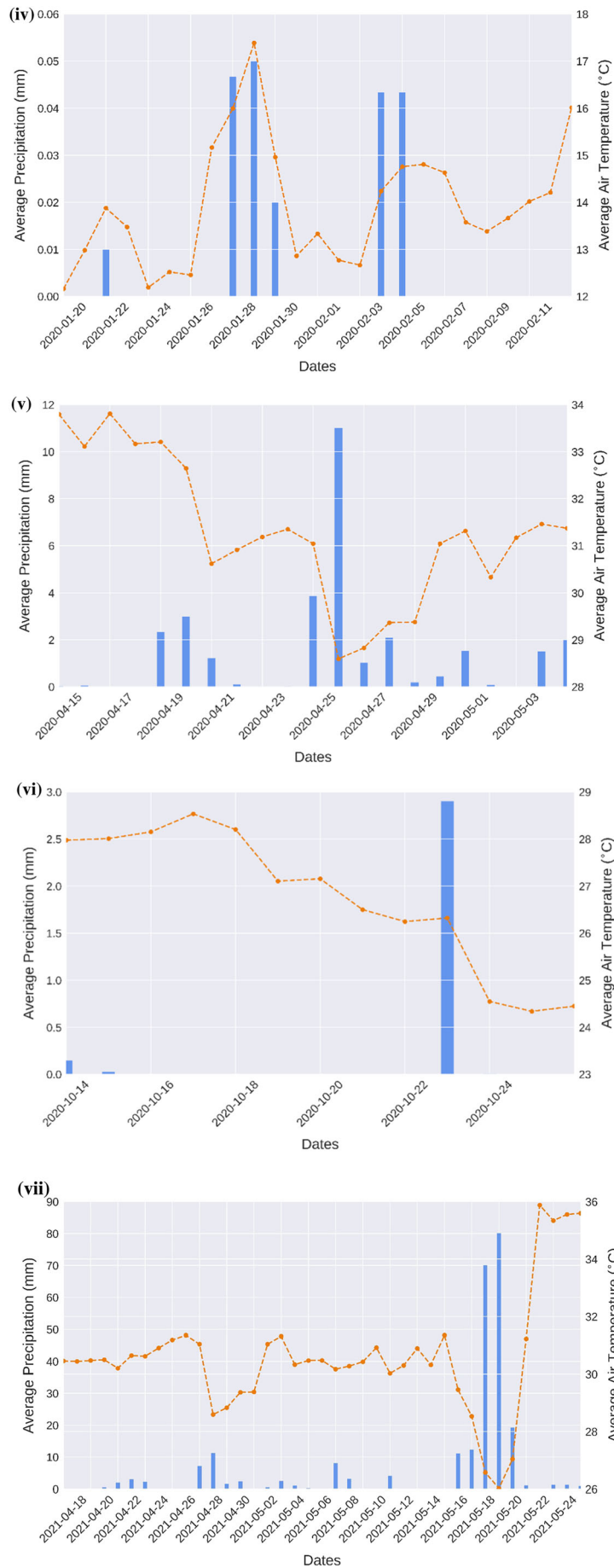
Figure 10. (*Continued.*)

difference maps (May 2020–February 2020) of the study stretches shows medium and low fluctuations. It can be due to coronavirus disease 2019 (COVID-19) during February 2020 that slowly started to take its toll in the entire country, and the anthropogenic activities near riverbanks had begun to decrease, therefore pH of the river begun to show signs of improvement. However in the Mirzapur region, some of the industries still remained open during February 2020, continuously discharging their industrial effluents into the river, which decreased the pH, so the difference map (May 2020–February 2020) showed some patches of high pH fluctuations. Even the difference map (May 2020–October 2020) of pH for Mirzapur stretch also shows some patches of high pH fluctuations, and the reason remains the same that during the post-lockdown period (October 2020), some of the industries again started to operate, and waste from industries caused a decrease in pH of the water. In the Ghazipur stretch, the difference map (May 2020–October 2020) shows some places to have high fluctuations in pH. In this region, illegal sand mining activities have been carried out at some places after lockdown, and sand mining can increase the metal concentration in the river (Duncan *et al.* 2018), which in turn can decrease the pH of the river water (Li *et al.* 2013). The DO difference map (May 2020–February 2020) for the considered stretches depicts that fluctuation of the DO has been in the range of mostly medium and high only at some sporadic places. These fluctuations can be attributed to the fact that during February 2020, people avoided visiting crowded places such as *ghats* (river banks), so the anthropogenic activities had begun to diminish, and thus enhanced the river DO gradually. From the difference map (May 2020–October 2020), it can be seen that DO fluctuation has become low and lower for all the areas of study because there were almost negligible anthropogenic activities and very less amount of industrial waste discharged into the river. After lockdown, the unlock process started in India in a phased manner, but most industries were still closed.

The suspended concentration or TSS has been closely related to turbidity, and they are treated on similar lines in the field of remote sensing (Ritchie *et al.* 2003). The difference map (May 2020–May 2019) of TSS depicts high fluctuation for all the study stretches. This can be attributed to the fact that during the lockdown (May 2020), turbidity has been reduced considerably as compared to May 2019, when everything was normal. For the difference map (May 2020–October 2020), the TSS fluctuation is very low. It is because due to lockdown and in the post-lockdown stage, the industries mostly remain closed, and even the anthropogenic activities were very minimal, so there is a little change in the suspended solid level of the river. The difference map (May 2020–February 2020) of TSS depicts the medium and high fluctuations. This is because some of the industries were still open in February 2020, and some anthropogenic activities had taken place on the riverbank, so there is some variation in the TSS.

4.3 *Analysis of the water quality parameter fluctuations due to lockdown imposed in the second wave of COVID-19 in summers of 2021*

In mid-March 2021, the second wave of COVID-19 had begun to spread its tentacles throughout the country. Then in the upcoming months, the situation turned from bad to worse. The major affected states in the second wave were Maharashtra, Kerala, Karnataka, Andhra Pradesh, Tamil Nadu, Delhi, Uttar Pradesh (UP) and West Bengal. In March 2020, the Indian central government had imposed a nationwide lockdown. However, health being a state issue as per the constitution of the country, in 2021, the central government had given the responsibility of lockdown to the respective states (Kar *et al.* 2021). As such, the UP government did not impose complete lockdown; instead, it opted for the weekend lockdown rule starting from 24th of April to 24th of May (YKA post 2021). Due to weekend lockdown, the industries were functional, and even the anthropogenic activities continued on the *ghats* of the river. The river turbidity value for the three considered stretches had been high in May 2021 as compared to May 2020. The industrial waste discharge and the anthropogenic activities near the *ghats* were some of the reasons for the inflated turbidity value. The temperature of the river had also been high in May 2021 as compared to May 2020. In the second half of May 2021, the river temperature increased further than first half of May 2021. This region received high precipitation from 18th to 20th May 2021, as shown in the meteorological parameter graph (figure 10vii),

but still, the river temperature on 23rd May 2021 has elevated values in comparison with 7th May 2021.

4.4 *Special emphasis for the Varanasi stretch*

Varanasi is one of the most populated cities and very famous for Vedic culture. The correlation graph, absolute thermal difference maps and the NDTI maps have been drawn specifically for this region only. This region is worst affected by polluted water of the river since a huge number of the population in this region depends on the river for numerous purposes. The aquatic ecosystem in this region has been hampered heavily due to anthropogenic and industrial activities. Moreover, in this stretch, two rivers Varuna and Assi, join the river Ganga and these rivers carry immense waste along with them. If the river restoration work is adequately performed in this region, then for the other areas of the considered stretch, it would not be a very tedious and a challenging task.

5. Conclusion

Satellite imageries have been used for the spatio-temporal analysis of the river water quality parameter in the considered study stretch for the pre-lockdown, lockdown and post-lockdown time period. A significant impact of the lockdown had taken place on the water quality of river Ganga in Varanasi and its nearby regions. In the Mirzapur stretch, the temperature of river Ganga decreased by 12.06% in May 2020 as compared to May 2019. Similarly, in Varanasi stretch, the temperature reduced by 8.62%, and in Ghazipur stretch, this decline of river temperature was noted as 7.14% in May 2020 as compared to May 2019. The decrease in the NDTI value showed a different trend. Varanasi showed the most significant decrease by 0.26 in May 2020 compared to that of May 2019. The reduction in the NDTI value was calculated by 0.24 in the Mirzapur stretch in May 2020 compared to May 2019. For the Ghazipur stretch, the decline of NDTI value was by 0.22 in May 2020 compared to May 2019. Several polluting industries had been closed, and the anthropogenic activities have also been reduced to a great extent due to the lockdown. After 4 weeks since the lockdown had begun, the production of essential items had been allowed by the government, and other industries were closed. So obviously, there had been less discharge and effluent generation. This situation has taken off the vast chunk of toxic load from the river. The water quality parameters have shown improvement, especially around the industrial clusters and urban areas. During the lockdown, the water quality of the river has shown progress, and it is evident that the leading cause of water quality degradation is anthropogenic factors. A significant reduction in the river turbidity was also very apparent. Grossly polluting industries in the river's catchment areas need to be regulated at the earliest because the water quality improvement due to the lockdown phenomenon is just a temporary reprieve. The river rejuvenation, observed during the first lockdown in the summer of 2020, had been deteriorating during the second wave lockdown (summer of 2021) in the UP region. In the second wave lockdown, the industries were not closed, and anthropogenic activities were also carried out, which increased the pollution level of the river. Necessary regulations should be implemented to reduce further deterioration of the water quality while considering the increasing rate of urbanisation and pollution load into the river. One of the biggest challenges will be to keep the river under similar conditions when life limps back to normal. The COVID-19 global pandemic is a once-in-a-generation occurrence that is currently plaguing the world. Nevertheless, it presents a similarly once-in-a-lifetime opportunity to redesign the existing frameworks and implement a robust as well as a dynamic mechanism to clean one of India's most polluted rivers and the other similarly afflicted watercourses of the nation.

Author statement

Conceptualisation: Nilendu Das, Rajarshi Bhattacharjee and Ashwani Kumar Agnihotri. Software: Abhinandan Choubey, Nilendu Das and Rajarshi Bhattacharjee. Methodology: Nilendu Das, Ashwani Kumar Agnihotri and Abhinandan

Choubey. Writing original draft: Rajarshi Bhattacharjee. Supervision: Dr Anurag Ohri and Dr Shishir Gaur. Reviewing and editing: Dr Anurag Ohri and Dr Shishir Gaur.

Availability of data and materials

Satellite datasets have been accessed through the GEE platform (https://earthengine.google.com) (accessed on 4–10 February 2021). Meteorological data have been prepared using POWER (The Prediction of Worldwide Energy Resource) datasets of NASA (https://power.larc.nasa.gov/data-access-viewer) (accessed on 15–17 February 2021).

References

Avdan U and Jovanovska G 2016 Algorithm for automated mapping of land surface temperature using Landsat 8 satellite data; *J. Sens.* **2016(2)** 1480307.

Baby J, Raj J S, Biby E T, Sankarganesh P, Jeevitha M V, Ajisha S U and Rajan S S 2010 Toxic effect of heavy metals on aquatic environment; *Int. J. Biol. Chem. Sci.* **4(4)** 939–952, https://doi.org/10.4314/ijbcs.v4i4.62976.

Barbieri T, Despini F and Teggi S 2018 A multi-temporal analyses of land surface temperature using Landsat-8 data and open source software: The case study of Modena, Italy; *Sustainability* **10(5)** 1678.

Bhattacharjee R, Choubey A, Das N, Ohri A and Gaur S 2020 Detecting the carotenoid pigmentation due to haloarchaea microbes in the Lonar lake, Maharashtra, India using Sentinel-2 images; *J. Indian Soc. Remote Sens.* **49(2)** 305–316.

Braga F, Scarpa G M, Brando V E, Manfè G and Zaggia L 2020 COVID-19 lockdown measures reveal human impact on water transparency in the Venice Lagoon; *Sci. Total Env.* **736** 139612.

Bresciani M, Cazzaniga I, Austoni M, Sforzi T, Buzzi F, Morabito G and Giardino C 2018 Mapping phytoplankton blooms in deep subalpine lakes from Sentinel-2A and Landsat-8; *Hydrobiologia* **824(1)** 197–214.

Brown G W and Krygier J T 1970 Effects of clear-cutting on stream temperature; *Water Resour. Res.* **6(4)** 1133–1139.

Caissie D 2006 The thermal regime of rivers: A review; *Freshwater Biol.* **51(8)** 1389–1406.

Chander S, Gujrati A, Hakeem K A, Garg V, Issac A M, Dhote P R, Kumar V and Sahay A 2019 Water quality assessment of river Ganga and Chilika lagoon using AVIRIS-NG hyperspectral data; *Curr. Sci.* **116(7)** 1172–1181.

Chauhan A and Singh R P 2020 Decline in $PM_{2.5}$ concentrations over major cities around the world associated with COVID-19; *Environ. Res.* **187** 109634.

Collivignarelli M C, Abbà A, Bertanza G, Pedrazzani R, Ricciardi P and Miino M C 2020 Lockdown for COVID-2019 in Milan: What are the effects on air quality?; *Sci. Total Environ.* **732** 139280.

CPCB (Central Pollution Control Board) 2020 Impact of lockdown on water quality of river Ganga, CPCB, Ministry of Environment, Forest and Climate Change, Govt. of India, New Delhi, https://cpcb.nic.in/openpdffile.php?id=TGF0ZXN0RmlsZS8yOTNfMTU4Nzk3ODU3MV9tZWRpYXBob3RvMTY3MDYucGRm.

Dantas G, Siciliano B, França B B, da Silva C M and Arbilla G 2020 The impact of COVID-19 partial lockdown on the air quality of the city of Rio de Janeiro, Brazil; *Sci. Total Env.* **729** 139085.

Das N, Ohri A, Agnihotri A K, Omar P J and Mishra S 2020 Wetland dynamics using geo-spatial technology; *Adv. Water Res. Eng. Manag.* **39** 237–244.

de Moraes Novo E M L, de Farias Barbosa C C, de Freitas R M, Shimabukuro Y E, Melack J M and Pereira Filho W 2006 Seasonal changes in chlorophyll distributions in Amazon floodplain lakes derived from MODIS images; *Limnology* **7(3)** 153–161.

Dong J, Xiao X, Menarguez M A, Zhang G, Qin Y, Thau D *et al.* 2016 Mapping paddy rice planting area in northeastern Asia with Landsat 8 images, phenology-based algorithm and Google Earth Engine; *Remote Sens. Environ.* **185** 142–154.

Doxaran D, Froidefond J M, Lavender S and Castaing P 2002 Spectral signature of highly turbid waters: Application with SPOT data to quantify suspended particulate matter concentrations; *Remote Sens. Env.* **81(1)** 149–161.

Duncan A E, de Vries N and Nyarko K B 2018 Assessment of heavy metal pollution in the sediments of the river Pra and its tributaries; *Water Air Soil Pollut.* **229(8)** 1–10.

Dwivedi A C, Mishra A S, Mayank P and Tiwari A 2016 Persistence and structure of the fish assemblage from the Ganga river (Kanpur to Varanasi section), India; *J. Geogr. Nat. Disast.* **6(159)** 2167–2587.

Eaton J G, McCormick J H, Goodno B E, O'brien D G, Stefany H G, Hondzo M and Scheller R M 1995 A field information-based system for estimating fish temperature tolerance; *Fisheries* **20(4)** 10–18.

Elachi C 1987 *Introduction to the physics and techniques of remote sensing*; Wiley, New York, Chapter 2.

El Din E S and Zhang Y 2017 Statistical estimation of the Saint John River surface water quality using Landsat-8 multi-spectral data; In: *ASPRS annual conference proceedings of imaging and geospatial technology forum (IGTF)*.

Garg V, Aggarwal S P and Chauhan P 2020 Changes in turbidity along Ganga river using Sentinel-2 satellite data during lockdown associated with COVID-19; *Geomatics Nat. Hazard. Risk* **11(1)** 1175–1195.

Garg V, Kumar A S, Aggarwal S P, Kumar V, Dhote P R, Thakur P K *et al.* 2017 Spectral similarity approach for mapping turbidity of an inland waterbody; *J. Hydrol.* **550** 527–537.

George J E, Aravinth J and Veni S 2017 Detection of pollution content in an urban area using Landsat 8 data; In: *International Conference on Advances in Computing, Communications and Informatics (ICACCI)*, IEEE, pp. 184–190.

Gholizadeh M H, Melesse A M and Reddi L 2016 A comprehensive review on water quality parameters estimation using remote sensing techniques; *Sensors* **16(8)** 1298.

Gillooly J F, Brown J H, West G B, Savage V M and Charnov E L 2001 Effects of size and temperature on metabolic rate; *Science* **293(5538)** 2248–2251.

Gorji T, Yildirim A, Hamzehpour N, Tanik A and Sertel E 2020 Soil salinity analysis of Urmia lake basin using Landsat-8 OLI and Sentinel-2A based spectral indices and electrical conductivity measurements; *Ecol. Indic.* **112** 106173.

Hamner S, Pyke D, Walker M, Pandey G, Mishra R K, Mishra V B *et al.* 2013 Sewage pollution of the river Ganga: An ongoing case study in Varanasi, India; *River Syst.* **3–4** 157–167.

Järvenpää M and Lindström K 2004 Water turbidity by algal blooms causes mating system breakdown in a shallow-water fish, the sand goby *Pomatoschistus minutus*; *Proc. Roy. Soc. London B: Biol. Sci.* **271(1555)** 2361–2365.

Joseph G 1996 Imaging sensors for remote sensing; *Remote Sens. Rev.* **13** 257–342.

Kachroud M, Trolard F, Kefi M, Jebari S and Bourrié G 2019 Water quality indices: Challenges and application limits in the literature; *Water* **11(2)** 361.

Kar S K, Ransing R, Arafat S Y and Menon V 2021 Second wave of COVID-19 pandemic in India: Barriers to effective governmental response; *EClinicalMedicine* **36** 1–2.

Kefford B J 1998 The relationship between electrical conductivity and selected macroinvertebrate communities in four river systems of south-west Victoria. Australia; *Int. J. Salt Lake Res.* **7(2)** 153–170.

Khattab M F and Merkel B J 2014 Application of Landsat 5 and Landsat 7 images data for water quality mapping in Mosul dam lake, Northern Iraq; *Arab. J. Geosci.* **7(9)** 3557–3573.

Klemas V, Borchardt J F and Treasure W M 1971 Suspended sediment observations from ERTS-1; *Remote Sens. Env.* **2** 205–221.

Kuhn C, de Matos Valerio A, Ward N, Loken L, Sawakuchi H O, Kampel M *et al.* 2019 Performance of Landsat-8 and Sentinel-2 surface reflectance products for river remote sensing retrievals of chlorophyll-a and turbidity; *Remote Sens. Env.* **224** 104–118.

Lacaux J P, Tourre Y M, Vignolles C, Ndione J A and Lafaye M 2007 Classification of ponds from high-spatial resolution remote sensing: Application to Rift valley fever epidemics in Senegal; *Remote Sens. Environ.* **106(1)** 66–74.

Lal P, Kumar A, Kumar S, Kumari S, Saikia P, Dayanandan A, Khan M L *et al.* 2020 The dark cloud with a silver lining: Assessing the impact of the SARS COVID-19 pandemic on the global environment; *Sci. Total Environ.* **732** 139297.

Lamaro A A, Mariñelarena A, Torrusio S E and Sala S E 2013 Water surface temperature estimation from Landsat 7 ETM+ thermal infrared data using the generalized single-channel method: Case study of Embalse del Río Tercero (Córdoba, Argentina); *Adv. Space Res.* **51(3)** 492–500.

Layman C A, Allgeier J E, Yeager L A and Stoner E W 2013 Thresholds of ecosystem response to nutrient enrichment from fish aggregations; *Ecology* **94(2)** 530–536.

Li H, Shi A, Li M and Zhang X 2013 Effect of pH, temperature, dissolved oxygen, and flow rate of overlying water on heavy metals release from storm sewer sediments; *J. Chem.* **2013** 104316, https://doi.org/10.1155/2013/104316.

Li L, Yang J and Wu J 2019 A method of watershed delineation for flat terrain using Sentinel-2a imagery and DEM: A case study of the Taihu basin; *ISPRS Int. J. Geo-Inf.* **8(12)** 528.

Ling F, Foody G M, Du H, Ban X, Li X, Zhang Y and Du Y 2017 Monitoring thermal pollution in rivers downstream of dams with Landsat ETM+ thermal infrared images; *Remote Sens.* **9(11)** 1175.

Luis K M, Rheuban J E, Kavanaugh M T, Glover D M, Wei J, Lee Z and Doney S C 2019 Capturing coastal water clarity variability with Landsat 8; *Mar. Pollut. Bull.* **145** 96–104.

Mahato S, Pal S and Ghosh K G 2020 Effect of lockdown amid COVID-19 pandemic on air quality of the megacity Delhi, India; *Sci. Total Environ.* **730** 139086.

Middelburg J J and Levin L A 2009 Coastal hypoxia and sediment biogeochemistry; *Biogeosci.* **6(7)** 1273–1293.

Montanaro M, Levy R and Markham B 2014 On-orbit radiometric performance of the Landsat 8 thermal infrared sensor; *Remote Sens.* **6(12)** 11,753–11,769.

Moore G K 1980 Satellite remote sensing of water turbidity/ satellite remote sensing of water turbidity; *Hydrol. Sci. J.* **25(4)** 407–421.

Muhammad S, Long X and Salman M 2020 COVID-19 pandemic and environmental pollution: A blessing in disguise?; *Sci. Total Environ.* **728** 138820.

Nasrabadi T, Ruegner H, Sirdari Z Z, Schwientek M and Grathwohl P 2016 Using total suspended solids (TSS) and turbidity as proxies for evaluation of metal transport in river water; *Appl. Geochem.* **68** 1–9.

Null S E, Mouzon N R and Elmore L R 2017 Dissolved oxygen, stream temperature, and fish habitat response to environmental water purchases; *J. Env. Manag.* **197** 559–570.

Orhan O and Yakar M 2016 Investigating land surface temperature changes using Landsat data in Konya, Turkey; *Int. Arch. Photogramm. Remote Sens. Spatial Inf.* **41** B8.

Otmani A, Benchrif A, Tahri M, Bounakhla M, El Bouch M and Krombi M H 2020 Impact of COVID-19 lockdown on PM_{10}, SO_2 and NO_2 concentrations in Salé city (Morocco); *Sci. Total Env.* **735** 139541.

Ouma Y O, Noor K and Herbert K 2020 Modelling reservoir chlorophyll-a, TSS, and turbidity using Sentinel-2A MSI and Landsat-8 OLI satellite sensors with empirical multi-variate regression; *J. Sens.* **2020** 8858408, https://doi.org/10.1155/2020/8858408.

Pahlevan N, Chittimalli S K, Balasubramanian S V and Vellucci V 2019 Sentinel-2/Landsat-8 product consistency and implications for monitoring aquatic systems; *Remote Sens. Environ.* **220** 19–29.

Pandey J and Singh R 2017 Heavy metals in sediments of Ganga river: Up- and downstream urban influences; *Appl. Water Sci.* **7(4)** 1669–1678.

Patel P P, Mondal S and Ghosh K G 2020 Some respite for India's dirtiest river? Examining the Yamuna's water quality at Delhi during the COVID-19 lockdown period; *Sci. Total Environ.* **744** 140851.

Pavelsky T M and Smith L C 2009 Remote sensing of suspended sediment concentration, flow velocity, and lake recharge in the Peace-Athabasca Delta, Canada; *Water Resour. Res.* **45(11)** 1–16.

Poirel A, Gailhard J and Capra H 2009 Influence of the management of reservoir dams on water temperature. Example of application to the Ain watershed; *SHF Proceedings: Low levels, droughts, rare heatwaves, and their impacts on water uses*, pp. 8–9.

Poole G C and Berman C H 2001 An ecological perspective on in-stream temperature: Natural heat dynamics and mechanisms of human-caused thermal degradation; *Environ. Manag.* **27(6)** 787–802.

Quang N H, Sasaki J, Higa H and Huan N H 2017 Spatiotemporal variation of turbidity based on Landsat 8 OLI in Cam Ranh bay and Thuy Trieu lagoon, Vietnam; *Water* **9(8)** 570.

Rai P K, Mishra A and Tripathi B D 2010 Heavy metal and microbial pollution of the river Ganga: A case study of water quality at Varanasi; *Aquat. Ecosyst. Health Manag.* **13(4)** 352–361.

Rai P K and Tripathi B D 2008 Heavy metals in industrial wastewater, soil and vegetables in Lohta village, India; *Toxicol. Environ. Chem.* **90(2)** 247–257.

Reuter D C, Richardson C M, Pellerano F A, Irons J R, Allen R G, Anderson M *et al.* 2015 The thermal infrared sensor (TIRS) on Landsat 8: Design overview and pre-launch characterization; *Remote Sens.* **7(1)** 1135–1153.

Ritchie J, Schiebe F R and McHenry J R 1976 Remote sensing of suspended sediments in surface waters; *Photogramm. Eng. Remote Sens.* **42(12)** 1539–1545.

Ritchie J C, Zimba P V and Everitt J H 2003 Remote sensing techniques to assess water quality; *Photogramm. Eng. Remote Sens.* **69(6)** 695–704.

Rongali G, Keshari A K, Gosain A K and Khosa R 2018 Split-window algorithm for retrieval of land surface temperature using Landsat 8 thermal infrared data; *J. Geovisualization Spat. Anal.* **2(2)** 1–19.

Rout C 2017 Assessment of water quality: A case study of river Yamuna; *Int. J. Earth Sci. Eng.* **10(2)** 398–403.

Roy D P, Wulder M A, Loveland T R, Woodcock C E, Allen R G, Anderson M C *et al.* 2014 Landsat-8: Science and product vision for terrestrial global change research; *Remote Sens. Env.* **145** 154–172.

Saravanan M 2020 Exploitation of artificial intelligence for predicting the change in air quality and rain fall accumulation during COVID-19; *Energy Sources A: Recovery Util. Environ. Eff.* **42** 1–10.

Sargaonkar A and Deshpande V 2003 Development of an overall index of pollution for surface water based on a general classification scheme in Indian context; *Environ. Monit. Assess.* **89(1)** 43–67.

Sebastiá-Frasquet M T, Aguilar-Maldonado J A, Santamaría-Del-Ángel E and Estornell J 2019 Sentinel 2 analysis of turbidity patterns in a coastal lagoon; *Remote Sens.* **11(24)** 2926.

Sekertekin A and Bonafoni S 2020 Land surface temperature retrieval from Landsat 5, 7, and 8 over rural areas: Assessment of different retrieval algorithms and emissivity models and toolbox implementation; *Remote Sens.* **12(2)** 294.

Sharma B, Kumar M, Denis D M and Singh S K 2019 Appraisal of river water quality using open-access earth observation data set: A study of river Ganga at Allahabad (India); *Sustain. Water Res. Manag.* **5(2)** 755–765.

Sharma Y C, Prasad G and Rupainwar D C 1992 Heavy metal pollution of river Ganga in Mirzapur, India; *Int. J. Environ. Stud.* **40(1)** 41–53.

Shukla N and Srivastava S (2020) *Lockdown impact: Ganga water in Haridwar becomes 'fit to drink' after decades.* India Today, https://www.indiatoday.in/india/story/lockdown-impact-ganga-water-in-haridwarbecomes-fit-to-drink-after-decades-1669576-2020-04-22.

Suarez M J, daSilva A, Dee D, Bloom S, Bosilovich M, Pawson S *et al.* 2005 Documentation and validation of the Goddard

Earth Observing System (GEOS) data assimilation system, version 4.

Subramaniam S and Saxena M 2011 Automated algorithm for extraction of wetlands from IRS Resourcesat LISS III data; *Int. Arch. Photogramm. Remote Sens. Spat. Inf. Sci.* **38(8/W20)** 193–198.

The Lancet 2020 India under COVID-19 lockdown; *Lancet (London, England)* **395(10233)** 1315.

Tornevi A, Bergstedt O and Forsberg B 2014 Precipitation effects on microbial pollution in a river: Lag structures and seasonal effect modification; *PLoS One* **9(5)** e98546.

Torres-Bejarano F, Arteaga-Hernández F, Rodríguez-Ibarra D, Mejía-Ávila D and González-Márquez L C 2020 Water quality assessment in a wetland complex using Sentinel 2 satellite images; *Int. J. Env. Sci. Technol.* **18** 2345–2356.

Trombadore O, Nandi I and Shah K 2020 Effective data convergence, mapping, and pollution categorization of ghats at Ganga river front in Varanasi; *Environ. Sci. Pollut. Res.* **27(1)** 15,912–15,924, https://doi.org/10.1007/s11356-019-06526-8.

Tyagi S, Sharma B, Singh P and Dobhal R 2013 Water quality assessment in terms of water quality index; *Am. J. Water Resour.* **1(3)** 34–38.

Vannote R L, Minshall G W, Cummins K W, Sedell J R and Cushing C E 1980 The river continuum concept; *Can. J. Fish. Aquat. Sci.* **37(1)** 130–137.

Vermote E, Justice C, Claverie M and Franch B 2016 Preliminary analysis of the performance of the Landsat 8/OLI land surface reflectance product; *Remote Sens. Env.* **185** 46–56.

Viswanathan V C, Molson J and Schirmer M 2015 Does river restoration affect diurnal and seasonal changes to surface water quality? A study along the Thur river, Switzerland; *Sci. Total Environ.* **532** 91–102.

Wawrzyniak V, Piégay H, Allemand P, Vaudor L, Goma R and Grandjean P 2016 Effects of geomorphology and groundwater level on the spatio-temporal variability of riverine cold water patches assessed using thermal infrared (TIR) remote sensing; *Remote Sens. Environ.* **175** 337–348.

Wawrzyniak V, Piégay H and Poirel A 2012 Longitudinal and temporal thermal patterns of the French Rhône river using Landsat ETM+ thermal infrared images; *Aquat. Sci.* **74(3)** 405–414.

Webb B W 1996 Trends in stream and river temperature; *Hydrol. Process.* **10(2)** 205–226.

Wurts W A and Durborow R M 1992 Interactions of pH, carbon dioxide, alkalinity and hardness in fish ponds; *SRAC Publ. No.* **464** 1–3.

Xin Z and Kinouchi T 2013 Analysis of stream temperature and heat budget in an urban river under strong anthropogenic influences; *J. Hydrol.* **489** 16–25.

Yadav N A, Ohri A and Das N 2020 Analysis of thermal pattern variation for river Ganges with satellite imagery; *J. Water Res. Eng. Manag.* **7(3)** 21–30.

YKA post 2021 *An Overview of the Catastrophic Second Wave in Uttar Pradesh*, https://www.youthkiawaaz.com/2021/07/an-overview-of-the-catastrophic-second-wave-in-uttar-pradesh.